Taylor & Francis
Taylor & Francis Group

Australian Journal of Earth Sciences
An International Geoscience Journal of the Geological Society of Australia

ISSN: (Print) (Online) Journal homepage: www.tandfonline.com/journals/taje20

Occurrence and petrogenesis of diverse S-type granites in an extensional tectonic setting: a case study from the Wongwibinda Complex, eastern Australia

K. Jessop, N. R. Daczko & S. Piazolo

To cite this article: K. Jessop, N. R. Daczko & S. Piazolo (02 Apr 2025): Occurrence and petrogenesis of diverse S-type granites in an extensional tectonic setting: a case study from the Wongwibinda Complex, eastern Australia, Australian Journal of Earth Sciences, DOI: 10.1080/08120099.2025.2476519

To link to this article: https://doi.org/10.1080/08120099.2025.2476519

AUSTRALIAN JOURNAL OF EARTH SCIENCES
https://doi.org/10.1080/08120099.2025.2476519

Occurrence and petrogenesis of diverse S-type granites in an extensional tectonic setting: a case study from the Wongwibinda Complex, eastern Australia

K. Jessop[a], N. R. Daczko[a] and S. Piazolo[b]

[a]Department of Natural Sciences, Macquarie University, Sydney, NSW, Australia; [b]School of Earth of Environment, Faculty of Environment, University of Leeds, Leeds, UK

ABSTRACT
The high-temperature–low-pressure (HTLP) Wongwibinda Metamorphic Complex (WMC) hosts four distinct types of early Permian S-type granitoids belonging, or related, to the Hillgrove Supersuite. We use field relationships, age data and petrogenetic modelling to determine the petrogenesis of these granitoid types. Biotite-only bearing granitoids are the most voluminous (~50% of the WMC area). A newly characterised second type (<1% of the WMC), here defined as the Wongwibinda monzogranite, has nearly equal proportions of muscovite and biotite, and a distinct chemical signature. The third and fourth types (<1% of the WMC) include pegmatite dykes and a garnet-bearing leucogranite. THERMOCALC modelling of water-fluxed and dehydration partial melting of local metasedimentary rock compositions indicates that the biotite-only granitoids are consistent with crustal melts produced by 30–40% dehydration partial melting of accretionary complex metasedimentary rocks at 6–9 kbar, with an admixture of ~30% mafic magma. In contrast, the Wongwibinda monzogranite is a nearly pure S-type granite with its composition influenced by assimilated migmatite xenoliths. One viable model for its geochemistry involves a mix of 45% water-fluxed 5–10% partial melt of metasedimentary rocks at 3–6 kbar, 65% assimilated local migmatites and inclusion of 10% residual biotite following the extraction of 20% haplogranite melt, although alternative scenarios are plausible. The leucogranite can be modelled through both dehydration and water-fluxed melting of metasedimentary rocks at 3–6 kbar, while the pegmatite composition is consistent with 5% water-fluxed or dehydration partial melts at 3 kbar. It is plausible that the pegmatites, leucogranite and Wongwibinda monzogranite formed coevally with peak metamorphism in the complex. In contrast, the emplacement of the biotite-only Hillgrove Supersuite plutons occurred in the later stages of thermal perturbation, as melts from the deep crust ascended *via* the Wongwibinda Shear Zone. Small volumes of two-mica Wongwibinda monzogranite type granitoids are commonly associated with HTLP metamorphism in extensional tectonic settings.

ARTICLE HISTORY
Received 25 November 2024
Accepted 3 March 2025

KEYWORDS
high-temperature–low-pressure metamorphism; pure S-type; hybridisation; two-mica granite; leucogranite; anatectic pegmatite; fluid-fluxed *vs* dehydration crustal anatexis; phase equilibrium

KEY POINTS

1. Four granitoid types are recognised within the WMC.
2. One is newly named and described.
3. Petrogenetic modelling and isotope data indicate that three are pure S-types formed from local metasedimentary rocks.
4. The most voluminous plutons are concluded to be a mix of S-type melts with minor mafic magma.

Introduction

Granites, a major component of Earth's upper continental crust, display a wide range of compositions, mineral assemblages and field relationships. They can form through various processes, including partial melting of crustal rocks, fractionation of more mafic magmas or a combination of partial melting, magma mixing, and fractionation (*e.g.* Brown *et al.*, 2016; Chappell & White, 1974; Fowler *et al.*, 2001; Johannes & Holtz, 2012). Partial melting can be driven by elevated temperatures causing dehydration melting or by the influx of fluids leading to water-fluxed melting (*e.g.* Weinberg & Hasalová, 2015). Over time, classification schemes for granites have evolved in tandem with increased understanding of their formation (Bonin *et al.*, 2020), although no single scheme is without limitations or universally accepted (García-Arias, 2020).

The S-I-M-A classification, developed in the early 1970s, remains one of the most widely used systems. In this scheme, S- and I-type granites are derived from the melting of supracrustal (sedimentary precursors that have experienced a weathering cycle) and infracrustal (igneous precursors that have not experienced a weathering cycle) protoliths,

CONTACT K. Jessop kim.jessop@mq.edu.au Department of Natural Sciences, Macquarie University, Sydney, NSW 2109, Australia
Supplemental data for this article can be accessed online at https://doi.org/10.1080/08120099.2025.2476519.
Editorial handling: Chris Fergusson

respectively (Appleby *et al.*, 2010; Chappell & White, 1974); A-type (anorogenic) granites typically form in rift zones, stable continental blocks, or post-collisional settings; and M-type granites, initially described as products of subducted oceanic crust melting at continental margins, have been redefined to include differentiated mafic magmas sourced from the mantle. Despite its recognised flaws (Bonin *et al.*, 2020), the classification of granitic rocks as S- or I-type is still prevalent, particularly in eastern Australia where the system originated (Bonin *et al.*, 2020; Chappell & White, 1974).

S-type granites can form *via* both water-fluxed and dehydration melting under a perturbed thermal gradient (*e.g.* Sawyer *et al.*, 2011; White & Chappell, 1988). These granites are common in the Paleozoic Gondwanan orogens (Tasmanides) of eastern Australia, where they are often associated with high-temperature–low-pressure metamorphic complexes (Collins & Richards, 2008; Jessop *et al.*, 2020). There is ongoing debate regarding the predominance of water-fluxed melting in granitoid formation complicated by the fact that criteria used to define water-fluxed melting can vary significantly between terranes (*e.g.* Gao & Zeng, 2014; Gao *et al.*, 2017; Li *et al.*, 2018).

This paper uses the Wongwibinda Metamorphic Complex (WMC) of the New England Orogen (NEO) as a case study to focus on the petrogenesis of different S-type granitoids with Aluminium Saturation Index (ASI) = 0.97–1.42. Metamorphism is confined to sedimentary rock of the Carboniferous accretionary wedge. We present results from updated field mapping, which identifies four types of granitoid: (1) Abroi Granodiorite and similar coeval plutons, (2) Wongwibinda monzogranite, (3) a leucogranite and (4) pegmatites. These granitoids are characterised by new XRF major- and trace-element, and isotope data.

The highest grade of metamorphism within the WMC is amphibolite facies with minor degrees of *in situ* melting, such that leucosomes within the migmatites are thought to have formed through injection of anatectic melts from deeper crustal levels (Binns, 1966; Farmer, 2017; Farrell, 1992; Jessop, 2017). This suggests that the WMC is part of a plutonic root complex where the Wongwibinda Shear Zone acts as a magma transfer conduit to feed plutons at the brittle–ductile crustal boundary (Brown, 2013). The four types of granitoid studied here occur within and/or on the edges of this zone.

The sedimentary rocks of the Carboniferous accretionary complex were deposited, buried and partially melted within 15 Myr (Jeon *et al.*, 2012). These rocks, being highly fertile, likely released significant amounts of aqueous fluid during metamorphism prior to partial melting. Therefore, it is plausible that melting may have involved both dehydration and water-fluxed styles.

The use of both melting experiments and phase equilibrium modelling has become increasingly important in the investigation of sources and emplacement histories of crustal plutons (*e.g.* Farina *et al.*, 2012; Garcia-Arias & Stevens, 2017a, 2017b; Koblinger & Pattison, 2017; Mayne *et al.*, 2020; Pavan *et al.*, 2021; Villaros, 2010; Zhang *et al.*, 2023). In the context of the Tasmanides, Li *et al.* (2021) employed thermodynamic modelling to compare melts from potential source rocks to the compositions of S-type granites of the Lachlan Orogen and determined that a mix of crustal and mantle sources are required to support the geochemistry. Based on whole-rock Sr and Nd isotopes, and zircon Hf isotopic data (Phillips *et al.*, 2011; Shaw *et al.*, 2011), Landenberger (1996) proposed a crustal–mantle mixing model for the Hillgrove Supersuite within the NEO. However, no supporting thermodynamic modelling studies have been conducted previously on granitoids within the NEO.

Measured compositions of various, representative metasedimentary rocks from the WMC were investigated using thermodynamic modelling software THERMOCALC (Holland & Powell, 2011; Powell *et al.*, 1998, 2005). We modelled the outcomes of water-fluxed *vs* dehydration partial melting of these rocks, and comparison of the modelled melt compositions with the chemistry of the granitoids allowed us to propose scenarios for the source of magmas that formed these local granitoids, their relationship to high-temperature–low-pressure metamorphism and the potential role of fluid-fluxed melting.

Regional geology

The WMC is located 45 km northeast of Armidale, New South Wales, Australia (Jessop *et al.*, 2020) and encompasses an area of approximately 340 km^2. It exhibits a progressive metamorphic grade from west to east, transitioning from sub-biotite grade to migmatites (Figure 1) defined by the occurrence of indicator minerals, from fine-grained biotite to muscovite porphyroblasts, K-feldspar and cordierite porphyroblasts, and finally to migmatites containing garnet and sillimanite. The WMC is one of a series of high-temperature–low-pressure metamorphic complexes in the NEO of eastern Australia containing granitoids that are interpreted to have formed through the melting of sedimentary rocks from the Carboniferous accretionary wedge (Flood & Shaw, 1977; Jessop *et al.*, 2020; Landenberger, 2001; Landenberger *et al.*, 2010; Shaw & Flood, 1981).

Accretionary rocks of the NEO (Figure 1, inset a) consist of slices of trench-wedge turbidites interleaved with oceanic basalt, deep-sea cherts and sediment that accumulated in front of the *ca* 360–305 Ma Currabubula-Connors continental arc (Cawood, 1982, 1983, 1984). During the following late Carboniferous to early Permian period of extension in the orogen (Rift phase: Jessop *et al.*, 2019; Korsch *et al.*, 2009), S-type granitoids of the Bundarra and Hillgrove supersuites, together with smaller mafic plutons of the Bakers Creek Supersuite (Bryant, 2017; Landenberger *et al.*, 2010), intruded the accretionary complex. The S-type granitoid supersuites are exposed in linear belts, with the relatively undeformed Bundarra Supersuite outcropping to the west (Figure 1, inset b). The Hillgrove Supersuite plutons in the east follow the pronounced curvature of major oroclines in the orogen and, in contrast, have experienced more significant deformation (Rosenbaum *et al.*, 2012). There is also a greater variety of compositions within the Hillgrove Supersuite, and they are linked exclusively with the mafic intrusions of the Bakers Creek Supersuite.

The WMC is bounded to the east by the north-north-west-trending Wongwibinda Fault, which dips westward beneath the metamorphic complex (Danis *et al.*, 2010). A broad zone of sheared rocks runs roughly parallel to the Wongwibinda

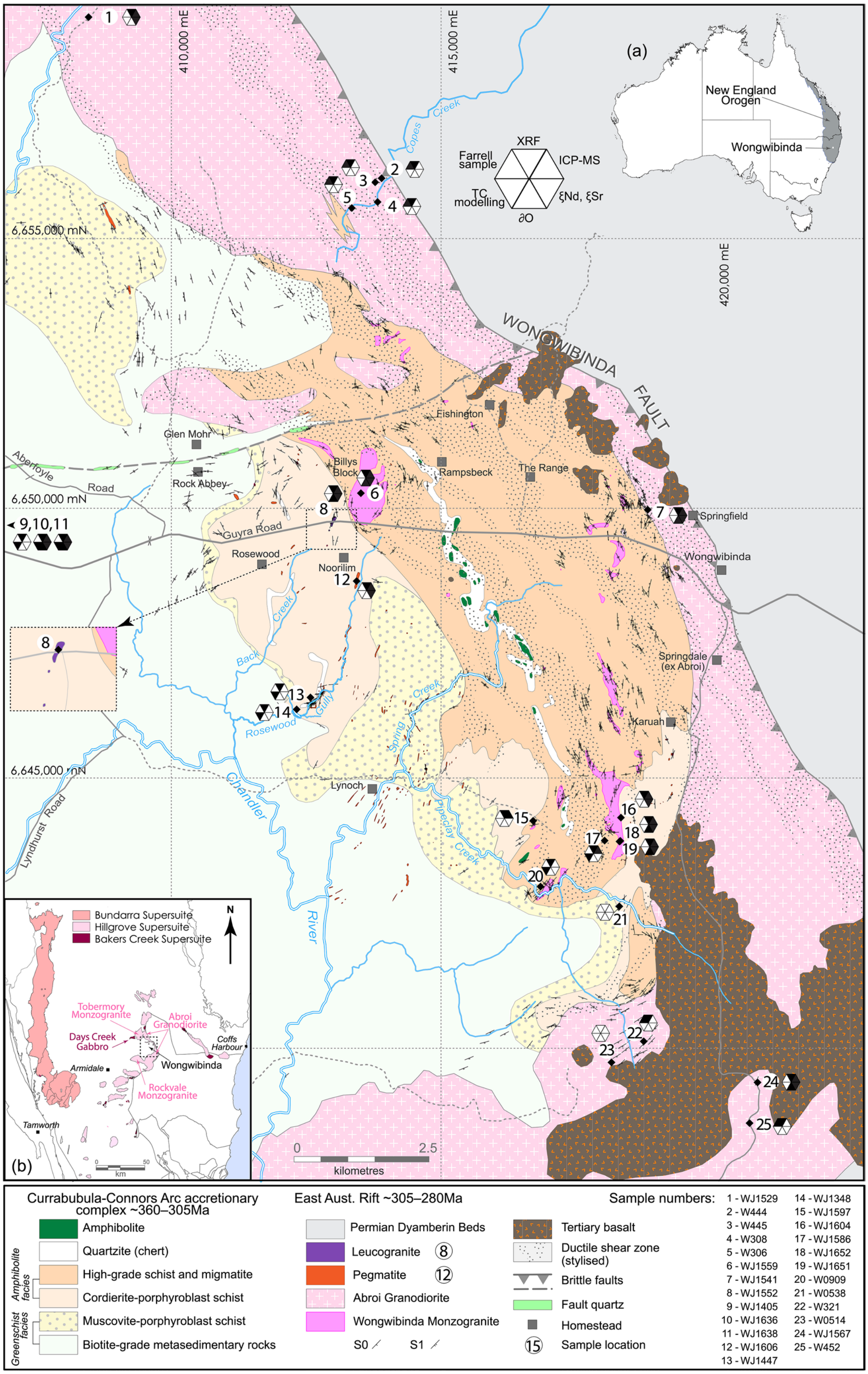

Figure 1. Geology of the Wongwibinda Metamorphic Complex showing sample locations and general structure. Inset (a): Location of Wongwibinda within the New England Orogen. Inset (b) Location of map in relation to outcrop of the Hillgrove (light pink) and Bundarra (dark pink) supersuites.

Fault (Figure 1). Although two parallel shear zones were previously designated in this area (Farrell, 1992), highly strained rocks and mylonites are widespread throughout the zone and do not clearly form two distinct bands. Consequently, a broad area of anastomosing high-strain zones within a 5 km-wide belt west of the Wongwibinda Fault is here proposed as the Wongwibinda

Shear Zone. The north–south extent of this shear zone has not been fully determined, although Farrell (1992) traced migmatites and sheared rocks adjacent to the Wongwibinda Fault for about 16 km to the north of the main complex. To the south, highly strained rocks disappear beneath Cenozoic basalt flows and curve westward under alluvial cover (Figure 1).

The complex is closely associated with granitoids, which cover up to 51% of the mapped area and is flanked on three sides by three biotite-only bearing plutons of the Hillgrove Supersuite. The Tobermory Monzogranite to the northwest (Figure 1, inset b) grades eastwards into the Abroi Granodiorite, which borders the complex to the east and southeast. Similarly, the Abroi Granodiorite transitions into the Rockvale Monzogranite to the southwest. New field mapping presented here (see details below, Figure 1) delineated dykes and small plutons of the two-mica Wongwibinda monzogranite within the highest-grade portions of the metamorphic complex. These outcrops were initially recognised by Farrell (1992) and to some degree by Binns (1966) but were mapped as components of the Abroi Granodiorite. Our study confirms that these two magmas have distinct geochemical signatures. Additional granitoid components comprise pegmatites and leucogranite. Pegmatites are abundant throughout the complex (Figure 1) and, although mapped by Farrell (1992), have not previously been subjected to geochemical analysis. A garnet-bearing leucogranite that differs from the other granitoids in the area has also been identified (Figure 1, location 8). We present new data regarding the composition of one pegmatite sample and one sample from the limited outcrop of leucogranite.

Geochronological constraints: data and general interpretations

A summary of dates for the Abroi Granodiorite, the Rockvale and Tobermory monzogranites, the Wongwibinda monzogranite, a pegmatite and selected migmatites is provided in Table 1 (Binns & Richards, 1965; Cawood *et al.*, 2011; Craven & Daczko, 2018; Craven *et al.*, 2012; Farrell, 1992; Jessop, 2017; Kent, 1994; Rosenbaum *et al.*, 2012). U–Pb studies on zircons and monazites by Craven *et al.* (2012) concluded that the Abroi Granodiorite crystallised after peak metamorphism (at 288.3 Ma), a hypothesis first proposed by Binns (1966). This interpretation is supported by field relationships, particularly the outcrop pattern of the Abroi Granodiorite in the southeastern part of the WMC (Figure 1, near location 23), where its boundary is perpendicular to metamorphic isograds in the surrounding metasedimentary rocks (Craven *et al.*, 2012). Similar zircon U–Pb dates have been reported for the Rockvale and Tobermory monzogranites.

Samples of the muscovite-rich Wongwibinda monzogranite were subjected to LA-ICPMS U–Pb dating (Jessop *et al.*, 2019), revealing no new zircon growth in the granitoid, although xenocrysts from the Carboniferous Currabubula–Connors arc are ubiquitous. Zircon rims, showing features, such as abundant porosity and inclusions, indicate partial modification and replacement of the zircon xenocrysts by coupled-dissolution-precipitation (CDP) (Asimus *et al.*, 2024). While ages obtained from the rims (290.6 ± 2 Ma and 301.7 ± 1.4 Ma) are concordant, they are not considered particularly reliable, given the limitations of dating zircon modified by CDP replacement

Table 1. Geochronological summary of the Wongwibinda Metamorphic Complex compiled from references listed.

Rock unit	Sample no.	Dating method	Age (Ma)	Error (Ma)	Reference
Abroi Granodiorite	WC38 (GA1300)	K/Ar biotite	252		Binns and Richards (1965)
Abroi Granodiorite	WC33 (GA1362)	K/Ar biotite	208		Binns and Richards (1965)
Abroi Granodiorite	NE8/05	U–Pb zircon	290.2	2.5	Cawood *et al.* (2011)
Abroi Granodiorite	NE74/07	U–Pb zircon	289.8	1.7	Cawood *et al.* (2011)
Abroi Granodiorite	W0514	U–Pb zircon	290.5	1.6	Craven and Daczko (2018); Craven *et al.* (2012)
Abroi Granodiorite	W0542	U–Pb zircon	298.9	2.7	Craven and Daczko (2018)
Abroi Granodiorite	W0603	U–Pb zircon	292.6	2.5	Craven and Daczko (2018)
Abroi Granodiorite	W0514	Monazite	288.3	5.4	Jessop (2017)
Abroi Granodiorite	W308	Rb/Sr biotite	261.9	1.4	Farrell (1992)
Abroi Granodiorite	W444	Rb/Sr coarse biotite	265.7	1.12	Farrell (1992)
Abroi Granodiorite	W444	Rb/Sr fine biotite	255.9	42	Farrell (1992)
Abroi Granodiorite	W445	Rb/Sr coarse biotite	260.7	0.61	Farrell (1992)
Abroi Granodiorite	W445	Rb/Sr fine biotite	256.8	15	Farrell (1992)
Wongwibinda monzogranite	WJ1559	U–Pb zircon	290.6	2	Jessop (2017)
Wongwibinda monzogranite	WJ1651	U–Pb zircon	301.7	1.4	Jessop (2017)
Wongwibinda monzogranite	WJ1559	U–Pb monazite	296.1	3.9	Jessop (2017)
Wongwibinda monzogranite	WJ1651	U–Pb monazite	288.4	5.0	Jessop (2017)
Wongwibinda monzogranite	W442	Rb/Sr coarse biotite	260.1	1.9	Farrell (1992)
Wongwibinda monzogranite	W442	Rb/Sr coarse muscovite	262.2	22	Farrell (1992)
Tobermory Monzogranite	NE1030	U–Pb zircon	292.4	2.9	Rosenbaum *et al.* (2012)
Tobermory Monzogranite	W0807	U–Pb zircon	295.9	1.9	Craven and Daczko (2018)
Rockvale Monzogranite		U–Pb zircon	303.0	3.0	Kent (1994)
Rockvale Monzogranite	NE75/07	U–Pb zircon	297.2	1.8	Cawood *et al.* (2011)
Rockvale Monzogranite	W0809	U–Pb zircon	293.8	3.3	Craven and Daczko (2018)
Pegmatite	W0538	U–Pb zircon	296.2	2.4	Craven and Daczko (2018)
Migmatite	WB71 (GA1360)	K/Ar biotite	253		Binns and Richards (1965)
Migmatite	W0501c	U–Pb monazite	295.7	2.4	Craven *et al.* (2012)
Migmatite	W0501d	U–Pb monazite	299.5	2.8	Craven *et al.* (2012)
Migmatite	W0503	U–Pb monazite	296.5	4.3	Craven *et al.* (2012)
Migmatite	WJ1650	U–Pb monazite	294.1	4.9	Jessop (2017)
Migmatite	WJ1656	U–Pb monazite	295.6	3.6	Jessop (2017)

(*e.g.* Daczko *et al.*, 2024; Spier *et al.*, 2024). The fact that the Wongwibinda monzogranite and the highest-grade migmatites are co-located in the WMC (Figure 1) suggests that the granite is roughly contemporaneous with the estimated peak of metamorphism (296.8 ± 1.5 Ma; Craven *et al.*, 2012).

Dating of the leucogranite (WJ1552) was attempted (Jessop, 2017), but very few zircon grains were extracted, and nearly all produced discordant spot dates. Four concordant grains gave a weighted average age of 330.2 ± 6.2 Ma, which likely represents xenocrystic material. No new zircon growth was observed on the rims.

The date of 296.2 ± 2.4 Ma obtained from a pegmatite (Figure 1, location 21) in the southwestern part of the WMC (sample W0538) by Craven and Daczko (2018) may suggest that its intrusion occurred slightly before the main pulse of granite emplacement, although a range of spot zircon dates from this sample means this cannot be considered definitive.

Younger Rb/Sr and K/Ar dates obtained from biotite and muscovite (Table 1) are most likely an overprint of the *ca* 265–230 Ma Hunter–Bowen orogenic phase of compression and uplift post-dating the main prograde WMC metamorphic and igneous activity (Jessop *et al.*, 2019).

Method summary

During a series of field campaigns between 2013 and 2016, field relationships were identified, data recorded and samples taken. Here, we present details of representative samples for which sample numbers and field locations are shown in Figure 1. Descriptions and geochemical analyses of all samples collected from the WMC are provided in the Supplemental data (File 2).

Representative samples from outcrops of Abroi Granodiorite, Wongwibinda monzogranite and leucogranite were analysed using a combination of petrological examination, major element XRF, trace-element ICPMS, and oxygen, strontium and neodymium isotope analysis. Excluding oxygen isotopes, a single sample of pegmatite underwent the same analyses. Mineral chemistry was characterised through SEM–EDS and EMP analyses conducted at Macquarie University and the University of Tasmania. To further investigate the origins of these rocks, THERMOCALC modelling was performed for seven metasedimentary rock samples to determine the compositions of partial melts produced under both dehydration and water-fluxed conditions. Detailed descriptions of the analytical methods and THERMOCALC modelling parameters are included in the Supplemental data (File 1).

Outcrop pattern and field relationships of the granitoids

Abroi Granodiorite

The Abroi Granodiorite forms a sinuous, ~40 km-long outcrop along the Wongwibinda Fault (Figure 1), where it exhibits significant shearing and local brecciation proximal to the fault. Outcrops range from large tors and whalebacks (Figure 2a, b) to smaller, elongated spires (Figure 2c). North and south of the metamorphic complex, the outcrop balloons westward, and the granodiorite shows moderate but less intense deformation.

Contacts between the Abroi Granodiorite and the adjacent migmatites vary from sharp to sheared and irregular. Within the shear zone, enclaves predominantly composed of strongly aligned biotite with subordinate fine-grained quartz and feldspar are common in the Abroi Granodiorite (Figure 2j). These enclaves are rarely observed in the less deformed portions of the pluton. Away from the shear zone, particularly around the associated Rockvale and Tobermory plutons, typical, intrusive contacts are evident between the metasedimentary rocks and the granitoids.

A distinct east–west elongated protrusion of Abroi Granodiorite outcrops from northwest of Fishington to immediately north of Glen Mohr homestead (Figure 1). The foliation in these outcrops strikes west in contrast to predominant northwest–southeast strike in the granitoid to the east (Farrell, 1992; Jessop, 2017).

Several small apophyses interpreted to belong to the Abroi Granodiorite are present within the migmatite zone, but their provenance appears more complex (see 'Mineral Assemblages' below). They are often located near outcrops of Wongwibinda monzogranite. Binns (1966) identified a small outcrop of 'Abroi Gneiss' north of Fishington, which contained garnet and was described as a 'marginal variant'.

To the northwest, the boundary between the Abroi Granodiorite and Tobermory Monzogranite is not well defined. A similar situation (Figure 2) occurs between the Abroi Granodiorite and Rockvale Monzogranite in the southwest (Jessop *et al.*, 2020).

Wongwibinda monzogranite

Previously referred to as the Wongwibinda granite (Jessop *et al.*, 2020), this unit has been reclassified as Wongwibinda monzogranite based on its geochemical signature (see below). Outcrops of Wongwibinda monzogranite are all closely associated with migmatites that occur exclusively within the Wongwibinda Shear Zone (Figure 1). Dykes and pods (<2 m across) of Wongwibinda monzogranite are scattered throughout the migmatites, with increasing abundance near small plutons (100 m to 1.5 km across). A characteristic 'lumpy' appearance (Figure 2e), caused by numerous migmatitic xenoliths and the weathering pattern influenced by the high mica (muscovite and biotite) content, is typical of these outcrops. This feature is less pronounced in the 'pavements' and 'whalebacks' found at the core of larger intrusions (Figures 1 and 2d).

A round pluton, approximately 1.5 × 0.5 km (0.75 km^2) in size, outcrops in the northwest of the complex on Billy's Block (Figure 1, location 6). This pluton lies within the 'Rock Abbey migmatite mass' referenced by Binns (1966) and lacks the strong deformation seen in the major pluton straddling the boundary between Lynoch and Karuah stations in the southeast of the complex (Figure 1, location 16). The latter, approximately 1.8 km × 0.33 km (0.6 km^2), is part of an elongated

Figure 2. Photographs of granitoid outcrops. (a–c) Abroi Granodiorite, (a) typical rounded boulders, (b) rounded whaleback, (c) strongly sheared 'spires'; (d–f) Wongwibinda monzogranite, (d) 'whalebacks', (e) typical 'lumpy' outcrop with numerous xenoliths, (f) a pavement showing complete mix of xenoliths of migmatite and Wongwibinda monzogranite; (g–i) pegmatites, (g) typical outcrop of large pegmatite dyke on Karuah Station, (h) smaller folded dyke in amphibolite facies metasedimentary rocks, (i) pegmatitic quartz in migmatites; (j) 'shlieren', biotite-rich enclaves in Abroi Granodiorite; (k) migmatite xenolith in Wongwibinda monzogranite; (l) quartz, feldspar and tourmaline in pegmatite; and (m) close-up of leucogranite; garnet is 2 mm across.

string of outcrops extending from Pipeclay Creek in the south to Springfield and The Range stations in the north. All these outcrops display post-emplacement deformation, primarily as strong foliation marked by mica alignment.

Small pods, likely of Wongwibinda monzogranite, have also been identified west and northwest of Fishington (Figure 1). This area has undergone significant brittle deformation associated with a late east–west-trending fault system (Figure 1), and the outcrops are highly weathered.

A gradation can be traced from the migmatites through diatexite into the Wongwibinda monzogranite. In the core of the largest monzogranite bodies, visible migmatite xenoliths make up approximately 5% of the rock, increasing progressively toward the edges to >50% (Figure 2f). Xenoliths within the Wongwibinda monzogranite retain the textures and compositions of migmatites and metasedimentary rocks (Figure 2k), differing significantly from the biotite-rich enclaves found in the Abroi Granodiorite. Rounded large quartz xenoliths, often arranged in trails, are also present within the Wongwibinda monzogranite and are possibly the remnants of quartz or pegmatite veins/dykes within the migmatites.

Pegmatites and leucogranite

Pegmatites are widespread throughout the lower-grade metasedimentary rocks of the WMC. Large, 2–4 m-wide, dykes (Figure 2g, l) are continuous over several to 100 m and generally oriented parallel to the dominant foliation. They form prominent outcrops, particularly between Spring Creek and Rosewood Gully (Figure 1, centred on Lynoch homestead). Within the migmatite zone, small, 20–50 cm-wide pegmatitic dykes and veins are abundant and exhibit deformation consistent with syn-tectonic injection (Figure 2h–i). A small occurrence of leucogranite (Figure 2m) crosses Guyra Road near the entrance to Noorilim (formerly Oakleigh) Station and has been traced into a nearby paddock (Figure 1, location 8). Although sparse, the outcrop suggests a dyke-like body with an approximate dyke thickness of 3 m.

General petrology and mineral assemblages

Abroi Granodiorite

Samples of Abroi Granodiorite from the main pluton display a consistent mineral assemblage, dominated by quartz, plagioclase, K-feldspar and biotite in clots in a typical igneous texture (Figure 3a1, a2; Table 2). Accessory minerals include apatite, ilmenite and zircon. In contrast, samples from small apophyses of Abroi Granodiorite within the migmatites sometimes contain minor muscovite and occasionally garnet. These apophyses usually occur in close proximity to outcrops of Wongwibinda monzogranite.

Wongwibinda monzogranite

The Wongwibinda monzogranite is distinct from the other S-type granites based on its significant primary muscovite content (Figure 3b1, b2; Table 2). Compared with the Abroi Granodiorite, the Wongwibinda monzogranite samples contain more than twice the total mica content and approximately half the amount of K-feldspar. Xenolith-free samples of monzogranite display predominantly igneous microstructure consisting of quartz, K-feldspar, plagioclase, biotite, muscovite and rare fine needles of ilmenite. However, even samples that appear free of xenoliths in hand specimen can contain evidence of partial assimilation of migmatite, as indicated by the presence of cordierite, sillimanite and garnet, along with their retrogressed products. As such, at the current outcrop level, it is extremely difficult to obtain a completely xenolith-free sample of the magma.

Fresh, possibly magmatic, euhedral cordierite has been observed in one sample, (WJ1597; Figure 3d1, d2), taken from a small intrusion of Wongwibinda monzogranite on Lynoch station, at its contact with migmatite (Figure 1, location 15). Conversely, retrogressed cordierite pseudomorphed by mats of muscovite and biotite, is commonly found in zones with partially assimilated xenoliths within the Wongwibinda monzogranite (Supplemental data, Figure S1a–d). Sillimanite typically appears as fine-grained dark (*i.e.* high relief) furry edges on feldspars, most often K-feldspar. It is also frequently found bordering myrmekite textures and within the spine of fibrous muscovite (Supplemental data, Figure S1e–h).

Leucogranite and pegmatites

The leucogranite has similar igneous microstructures to the Abroi and Wongwibinda granitoids. It is composed primarily of quartz, K-feldspar, plagioclase, muscovite, fine disseminated pink garnet, and traces of biotite (Figure 3c1, c2; Table 2). The muscovite content is similar to the Wongwibinda monzogranite (14 modal%) but K-feldspar is increased (30 modal%). Pegmatites are predominantly composed of very coarse-grained quartz, plagioclase and K-feldspar, and frequently contain tourmaline and occasionally garnet and/or muscovite (Figure 2l).

Table 2 presents the major mineral modes calculated by image analysis using ImageJ for a representative low-strain sample of Abroi Granodiorite (W0514, location 23) from the southern part of the main pluton, two samples of Wongwibinda monzogranite—one from the Billy's Block pluton (WJ1559, location 6) and the other from the Lynoch-Karuah pluton (WJ1651, location 19)—and one sample of leucogranite (WJ1552, location 8). Sample locations are shown in Figure 1.

Geochemistry

We supplement our data with unpublished data on the Abroi Granodiorite (Farrell, 1992) and the Hillgrove and Bundarra supersuites (Landenberger, 1996). Published data from Flood and Shaw (1977), Shaw and Flood (1981), Hensel *et al.* (1985), McKibbin (2006) and the Chappell database (Chappell unpublished data, preliminary CHAPGRAN dataset, C. Bryant pers. comm.) provide further context for the plutons of the Wongwibinda area (Supplemental data, File 2).

In addition, representative data from metasedimentary rocks and migmatites (Jessop, 2017) are used as a reference against which the granitoid data are compared to explore potential source rocks. Data for major and trace elements, as well as Sr, Nd and O isotopes, are provided in the Supplemental data (File 2).

Isotope data from other Hillgrove, Bundarra and Bakers Creek Supersuite samples (Flood & Shaw, 1977; Hensel *et al.*, 1985; Landenberger, 1996; McKibbin, 2006) are included for comparison.

Major elements

Major-element plots for the WMC granitoids (this study) and other coeval Hillgrove and Bundarra Supersuite plutons, with

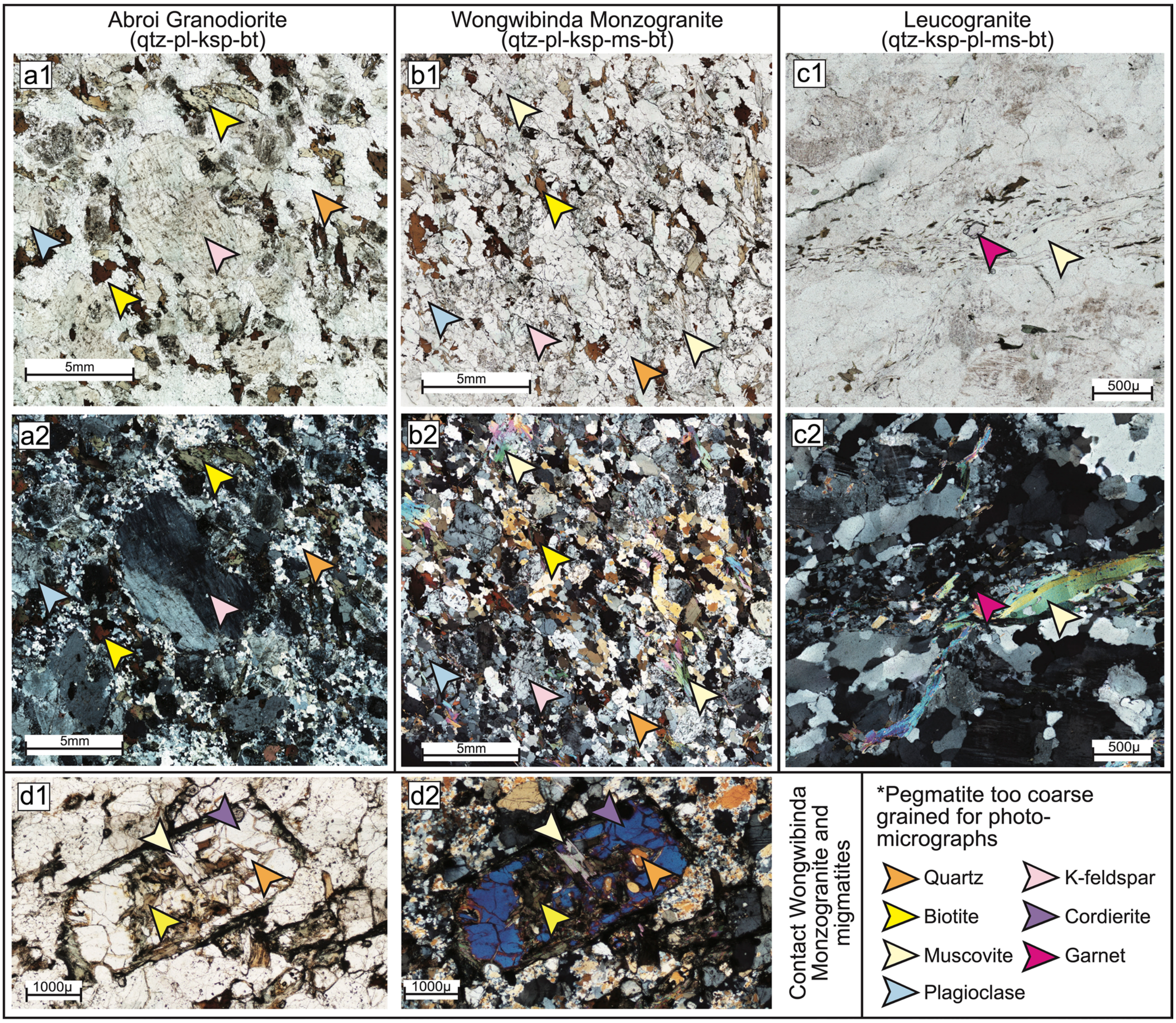

Figure 3. Granitoid photomicrographs (a1) plane-polarised light (PPL) and (a2) crossed polarised light (XPL): Abroi Granodiorite sample W0514, large K-feldspar (ksp) with biotite (bt), quartz (qtz) and plagioclase (pl). (b1) PPL and (b2) XPL: Wongwibinda monzogranite sample WJ1651. (c1) PPL and (c2) XPL of leucogranite sample WJ1552. (d1) PPL and (d2) XPL sample WJ1542, partly fresh igneous cordierite (crd) retrogressed to muscovite (ms), biotite (bt) and quartz (qtz).

Table 2. Mineral modes of WMC granitoids calculated using ImageJ.

Mineral	Abroi Granodiorite, Miragulee W0514	Wongwibinda monzogranite, Billy's Block WJ1559	Wongwibinda monzogranite, Lynoch-Karuah WJ1651	Leucogranite WJ1552
Quartz %	42	40	33	33
K-feldspar %	22	12	9	30
Plagioclase %	26	23	24	20
Biotite %	10	12	31	2
Muscovite %	–	13	7	14
Garnet %	–	–	–	1
Total mica %	10	25	38	16

the exception of P_2O_5, reveal similar fractionation trends for the Hillgrove and Bundarra supersuites, and divergent patterns for the Wongwibinda monzogranite (Figure 4). An inset for magnesium showing some samples from the Bakers Creek Supersuite is included to show the general relationship with the Hillgrove Supersuite. Although there is overlap between the Bundarra and Hillgrove supersuites, the Bundarra plutons tend to higher silica and the Hillgrove to lower silica.

The Abroi Granodiorite, together with the Tobermory and Rockvale monzogranites, exhibit compositions consistent with the broader Hillgrove Supersuite. In contrast, the Wongwibinda monzogranite is on average more mafic and has higher aluminium, iron and magnesium, and lower sodium at equivalent silica concentrations than the Abroi Granodiorite. The two granitoids also differ significantly in calcium and potassium concentrations, with the Wongwibinda

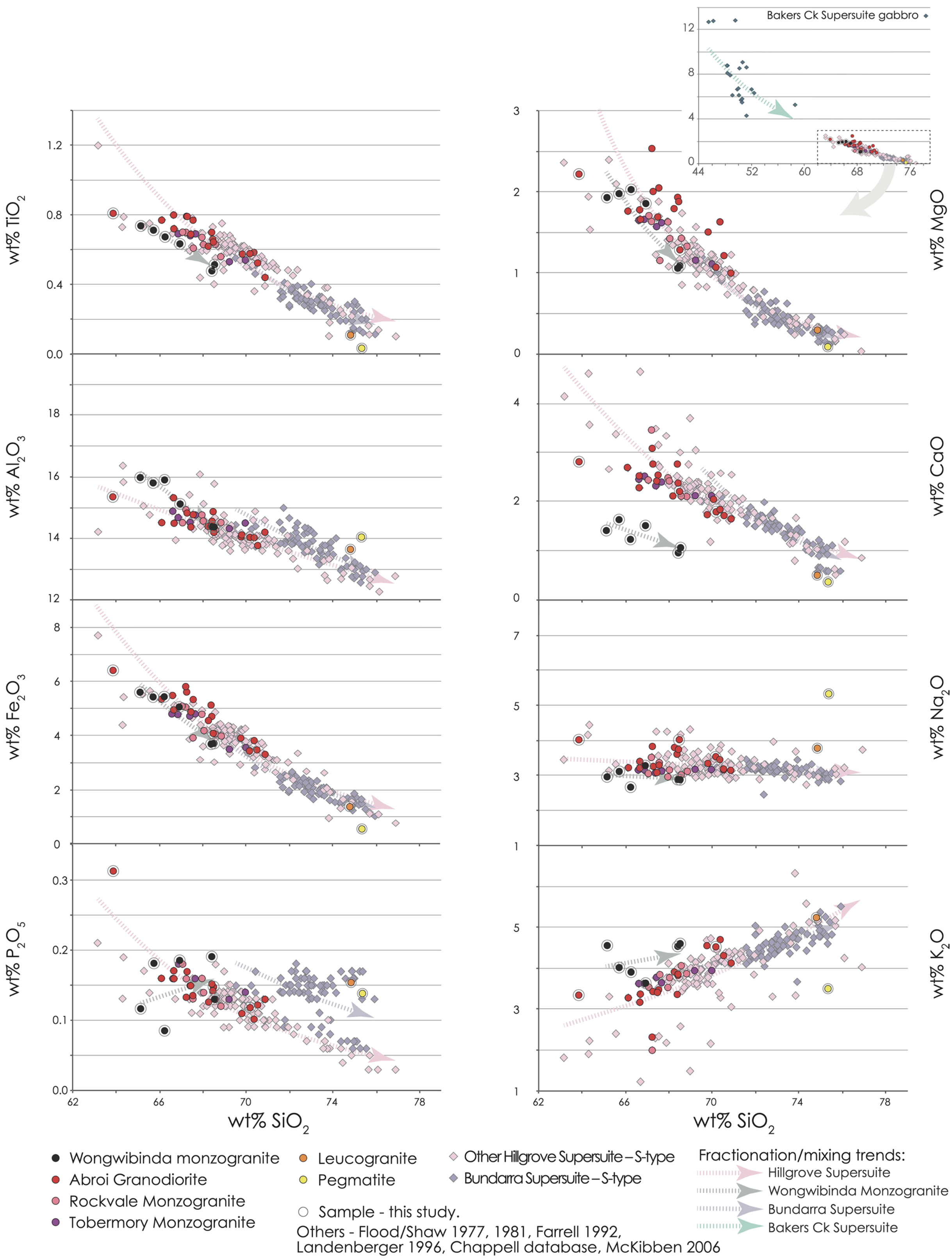

Figure 4. (a) Harker diagrams for all granitoids showing fractionation/mixing trends generated in Excel. Data from this study and other sources listed in the text. The Hillgrove and Bundarra supersuites follow a similar trend with the exception of P_2O_5 and to some degree Al_2O_3. The leucogranite is on the same trend with the exception of P_2O_5 and possibly Al_2O_3 and CaO. The pegmatite is generally off trend and the Wongwibinda monzogranite is mostly off trend, particularly for CaO, Al_2O_3 and K_2O. Inset shows how Bakers Creek Supersuite rocks relate to the Hillgrove and Bundarra supersuites using MgO as an example. Note: Trace-element data for the Hillgrove and Bundarra supersuites diverge, indicative of variations in the source rocks (Bryant, 2017), but both supersuites are shown, as they are coeval.

monzogranite having a lower calcium and higher potassium content.

Samples from both the Abroi and Wongwibinda granitoids fall within the compositional range of local WMC metasedimentary rocks (Supplemental data, Figure S2). These metasedimentary rocks are categorised into two groups based on metamorphic grade: those that experienced metamorphism above the aluminosilicate-in isograd are classified as amphibolite facies, while those below it are designated as greenschist facies. This classification is also reflected in their geochemistry, with greenschist facies rocks largely preserving the bulk composition of their sedimentary protoliths, whereas amphibolite facies rocks often show evidence of metasomatic alteration (Jessop, 2017). These two geochemical groups are examined as potential source rocks for the generation of S-type granite melts in the thermodynamic models that follow.

There is some tendency for the Wongwibinda monzogranite to plot near the amphibolite facies rocks and for the Abroi Granodiorite to associate with the greenschist facies rocks. Figure S2 (Supplemental data) plots all available major-element data for the metasedimentary rocks in the Wongwibinda area (Craven, 2015; Danis, 2007; Farrell, 1992; Jessop, 2017; Stuart, 2012; Teague, 2010).

The leucogranite and pegmatite are generally more siliceous than, and somewhat distinct from, the metasedimentary rocks (Supplemental data, Figure S2). The leucogranite is chemically similar to the more siliceous members of the Hillgrove Supersuite but resembles the Bundarra Supersuite granitoids in phosphorus content, possibly owing to the high solubility of phosphorus in peraluminous melts (Figure 4).

The pegmatite displays a similar but more extreme pattern to the leucogranite, being significantly higher in sodium and lower in potassium.

Trace elements

The four granitoid types have distinct rare earth element (REE) profiles despite the Abroi Granodiorite, leucogranite and pegmatite having similar slopes (Figure 5a, inset 1). The Wongwibinda monzogranite and Abroi Granodiorite differ in the shape of the middle REE (MREE)—heavy REE (HREE) profiles and the scale of their Eu anomalies (Figure 5a). The Abroi Granodiorite shows a higher HREE and a pronounced negative Eu anomaly (average Eu/Eu* = 0.50), while the Wongwibinda monzogranite has a lower HREE and a weak Eu anomaly (average Eu/Eu* = 0.77). Comparisons between the granitoids with greenschist and amphibolite facies metasedimentary rocks show a strong similarity between the amphibolite facies rocks (average Eu/Eu* = 0.72) and the Wongwibinda monzogranite, whereas the profile of the Abroi Granodiorite overlaps with greenschist facies rocks with the exception of Eu (average Eu/Eu* = 0.73 for greenschist facies rocks). The leucogranite is depleted in light to middle REEs compared with the Abroi Granodiorite and Wongwibinda monzogranite, although its HREE content overlaps with that of the Wongwibinda monzogranite. It has an Eu anomaly comparable with that of the Abroi Granodiorite (Eu/Eu* = 0.51). The pegmatite is significantly more depleted in all REEs than the other granitoids and displays an extreme Eu anomaly (Eu/Eu* = 0.06).

Regarding high-field-strength (HFS) and large-ion lithophile (LIL) elements, the Wongwibinda monzogranite shows higher Ba, U and K, and lower Ce, Dy, Y, Yb and Lu than the Abroi Granodiorite (Figure 5b). Notably, both granitoids have a lower Zr than the greenschist facies metasedimentary rocks. The leucogranite and pegmatite exhibit generally lower values of LIL and HFS elements than other granitoids and host rocks. However, their Cs, Rb, U, K, Pb and P overlap with those from the Abroi and Wongwibinda plutons. Additionally, the leucogranite values for Zr, Ti and Y are similar to those for the Wongwibinda monzogranite and the migmatites.

The significantly higher K and Ba whole-rock values for the Wongwibinda monzogranite in relation to the Abroi Granodiorite may indicate there is significantly more K-feldspar/muscovite/biotite in the Wongwibinda monzogranite than has been calculated from modal assessment of thin-sections.

Isotopes

$^{143}Nd/^{144}Nd$ ratios are highest in the Abroi Granodiorite and the Hillgrove Supersuite in general, and fall outside the range of metasedimentary rock values (Figure 6a). In contrast, the Wongwibinda monzogranite and leucogranite show neodymium isotopic compositions consistent with the metasedimentary rocks, particularly those of higher metamorphic grade. The pegmatite and leucogranite exhibit significantly higher measured $^{87}Sr/^{86}Sr$ ratios than the granitoids and metasedimentary rocks (Figure 6a, inset).

Published data from Hensel *et al.* (1985) have significantly lower $^{143}Nd/^{144}Nd$ ratios than the other data sets, although accompanying εNd values are comparable. This discrepancy cannot be explained, and we applied a factor of 1.00157 to the $^{143}Nd/^{144}Nd$ values in order to replicate the published εNd.

Applying an age of 285 Ma to our data reveals a tight mixing line from the more crustal Wongwibinda monzogranite and leucogranite through the Abroi Granodiorite and pegmatite towards the mantle array. Applying initial ages between 292 Ma and 285 Ma for all plutonic suites produces only minor shifts. Initial values (εNd and $^{87}Sr/^{86}Sr$) shown in (Figure 6b) are based on an age of 285 Ma applied to all available plutonic data.

The Abroi Granodiorite groups with other Hillgrove Supersuite and Bundarra Supersuite samples that cluster northwest of Bulk Silicate Earth (Landenberger *et al.*, 2010). The Bakers Creek Supersuite samples overlap the Hillgrove Supersuite values and show a complex mixing trend towards depleted mantle.

For $\delta^{18}O$, the Abroi Granodiorite (10.7–11.4) and other Hillgrove plutons (10.35–11.82, Flood & Shaw, 1977) fall within the S-type granitoid range (Figure 6c). In contrast, the Wongwibinda monzogranite shows significantly higher $\delta^{18}O$ values (13.1–13.5), grouping towards the higher end of the metasedimentary rock range. The leucogranite has a $\delta^{18}O$ value (13.3) similar to the Wongwibinda monzogranite. Applying the

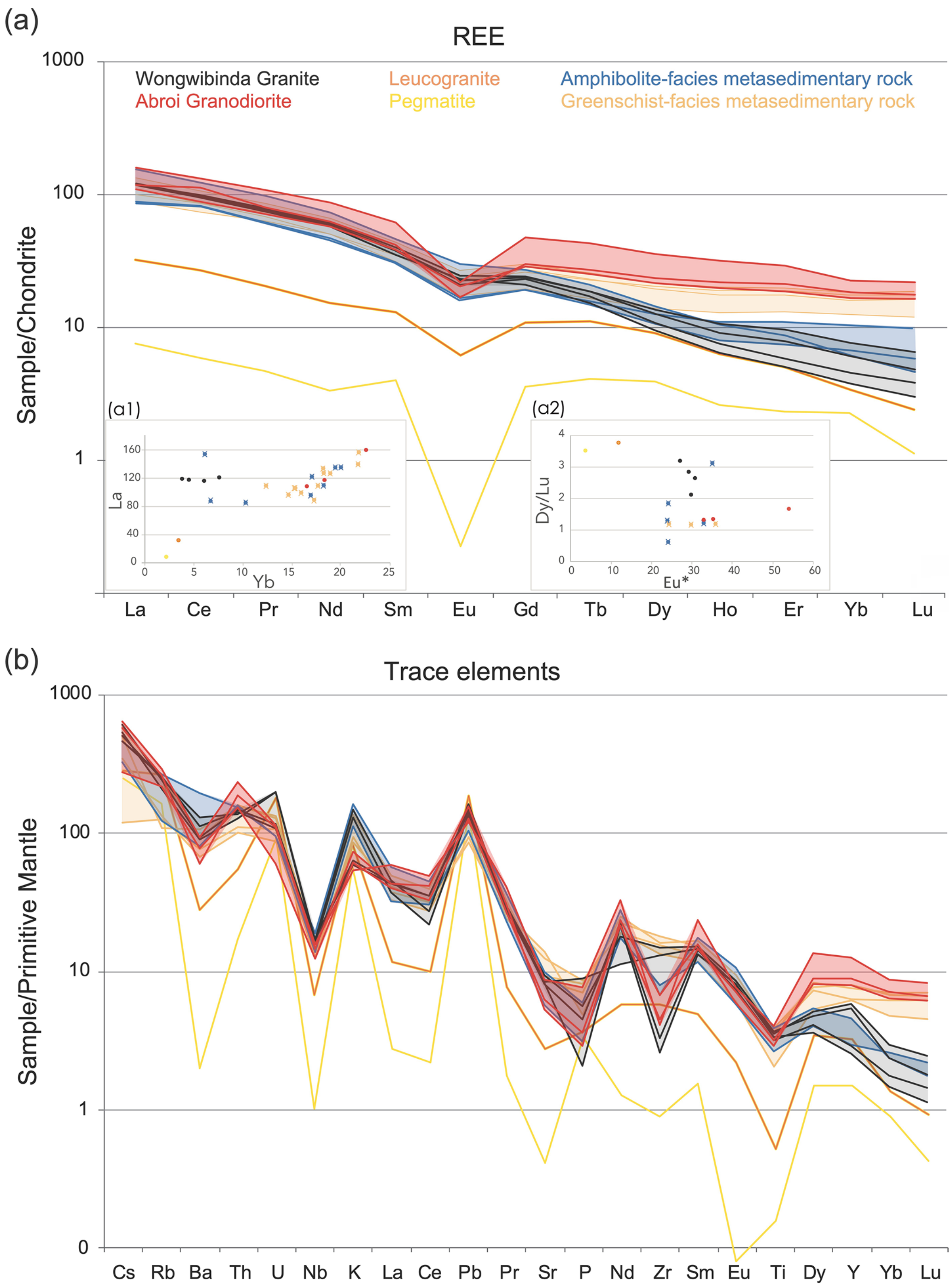

Figure 5. Trace elements. (a) REE: the Wongwibinda monzogranite has a similar REE pattern to amphibolite facies metasedimentary rocks with both having depleted heavy REE. The Abroi Granodiorite and greenschist facies metasedimentary rocks have similar patterns. The leucogranite and pegmatite have progressively more depleted REE patterns although the HREE of the leucogranite mimics that of the Wongwibinda monzogranite. There is a weak Eu anomaly in the metasedimentary rocks and the Wongwibinda monzogranite, a moderate anomaly in the Abroi Granodiorite and leucogranite and a significant anomaly in the pegmatite. Inset (a1) plots La against Yb and shows how the slope of the Wongwibinda monzogranite and some of the amphibolite facies metasedimentary rocks diverge from the other rocks. Inset (a2) More variation is apparent in a plot of Dy/Lu against Eu*, but again the difference between the granitoids is apparent (Note: fewer metasedimentary rocks were analysed for the full range of REE elements). (b) Spider diagram: The Abroi Granodiorite and Wongwibinda monzogranite differ for U, K and Dy–Lu. The Abroi has higher Dy–Lu and lower U and K. Both the Abroi and Wongwibinda granitoids are lower in Zr than the metasedimentary rocks but again, trace-element values for the Abroi more closely follow those of the greenschist facies metasedimentary rocks and those of the Wongwibinda monzogranite are closer to those of the amphibolite facies rocks. The leucogranite and pegmatite are depleted in most elements in comparison with the other granitoids with the exception of Cs, Rb, U, K, Pb, P. In addition, the leucogranite has similar values to the Wongwibinda monzogranite for Zr and Dy–Lu.

same initial age of 285 Ma for $^{87}Sr/^{86}Sr$ (Figure 6d) produces a grouping of the leucogranite with the Wongwibinda monzogranite at the more sedimentary range of volcaniclastic rocks, while the Abroi Granodiorite, other Hillgrove Supersuite and Bundarra Supersuite rocks trend from volcaniclastics towards values typical of ophiolitic basalts.

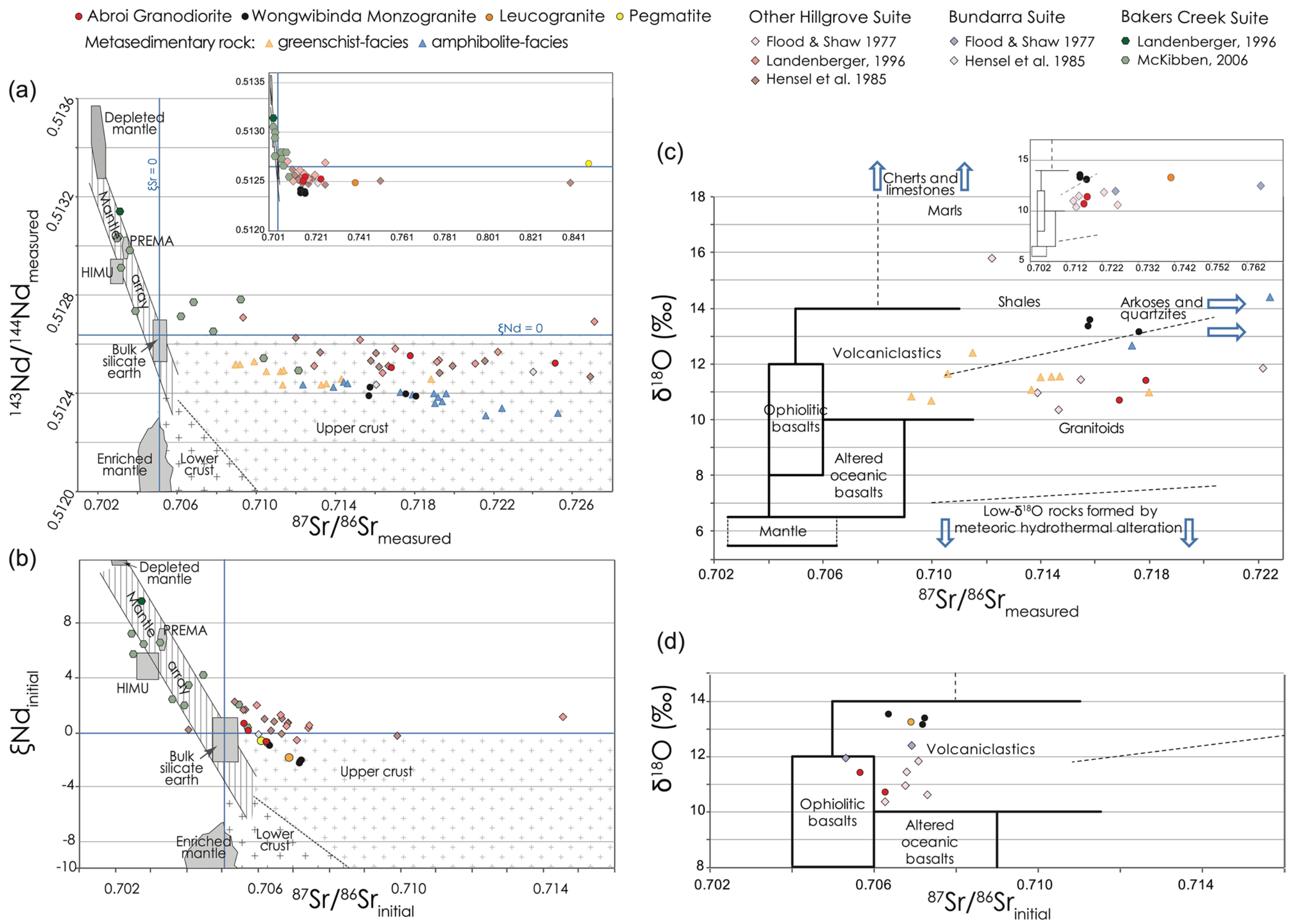

Figure 6. Isotope data. (a) Comparison of measured $^{143}Nd/^{144}Nd$ and $^{87}Sr/^{86}Sr$ isotopes showing consistency of Wongwibinda monzogranite with the metasedimentary rocks, increased mafic component of the Abroi Granodiorite, and overlaps with the Bakers Creek Supersuite rocks. Inset shows increased $^{87}Sr/^{86}Sr$ isotope ratios in the leucogranite and pegmatite. (b) Relationship of granitoid samples with an initial age of 285 Ma applied. (c) δ^{18}O of selected metasedimentary rocks, Abroi Granodiorite, other Hillgrove Supersuite and Wongwibinda monzogranite. Inset includes the leucogranite and Bundarra Supersuite rocks. (d) Grouping of samples with initial age of 285 Ma applied.

Thermodynamic modelling to explore granitoid sources and melting scenarios

General procedure

Scenarios for the formation of apparently coeval granitoids with varying geochemistry have been explored previously (*e.g.* Clemens, 2014; Clemens & Stevens, 2012; Farina *et al.*, 2012; Patiño Douce & Harris, 1998). However, the development of thermodynamic models provides a new tool to explore different crustal melting regimes and source compositions (*e.g.* Garcia-Arias & Stevens, 2017a, 2017b; Li *et al.*, 2021; Pavan *et al.*, 2021).

We explore the potential sources and melting scenarios of the four studied granitoids of the WMC specifically focusing on the potential role of melt contribution from local metamorphic rocks, deeper mantle sources and metasomatism through assimilation. In contrast to previous studies, which rely on standard or average rock compositions for modelling, this study utilises seven samples of metasedimentary rocks from the WMC as input into THERMOCALC modelling (for further details on technique, see the Supplemental data, File 1). In addition, we explore the two end-member scenarios of water-fluxed and dehydration melting.

The samples selected for modelling cover the two metamorphic groups: (i) greenschist facies, fine- and coarse-grained biotite and biotite–muscovite schists (WJ1405, WJ1636 and WJ1638), and (ii) amphibolite facies cordierite, cordierite–spessartine and cordierite–almandine schists/migmatite (WJ1348, W0909A, WJ1447 and WJ1586) (Figure 1). Major- and trace-element data, isotope values and modelled melt compositions for each sample are provided in Supplemental data (File 3). Pseudosections were developed for both dehydration and water-fluxed melting in a closed system between 450 and 900 °C and between 0.5 and 12 kbar (Figure 7 and Supplemental data, Figure S3a, b). Melt compositions were extracted at pressures of 3, 6, 9 and 12 kbar, and for melt fractions of 5%, 10%, 20%, 30%, 40% and 50%, wherever possible within the defined pressure–temperature (P/T) conditions.

To facilitate direct comparison between THERMOCALC derived melt compositions and granitoids, all granitoid and metasedimentary rock compositions in Figure 8 and Figure S4a, b (Supplemental data) have been normalised to exclude Ti, Mn, P and H_2O, referred to as TC-normalised.

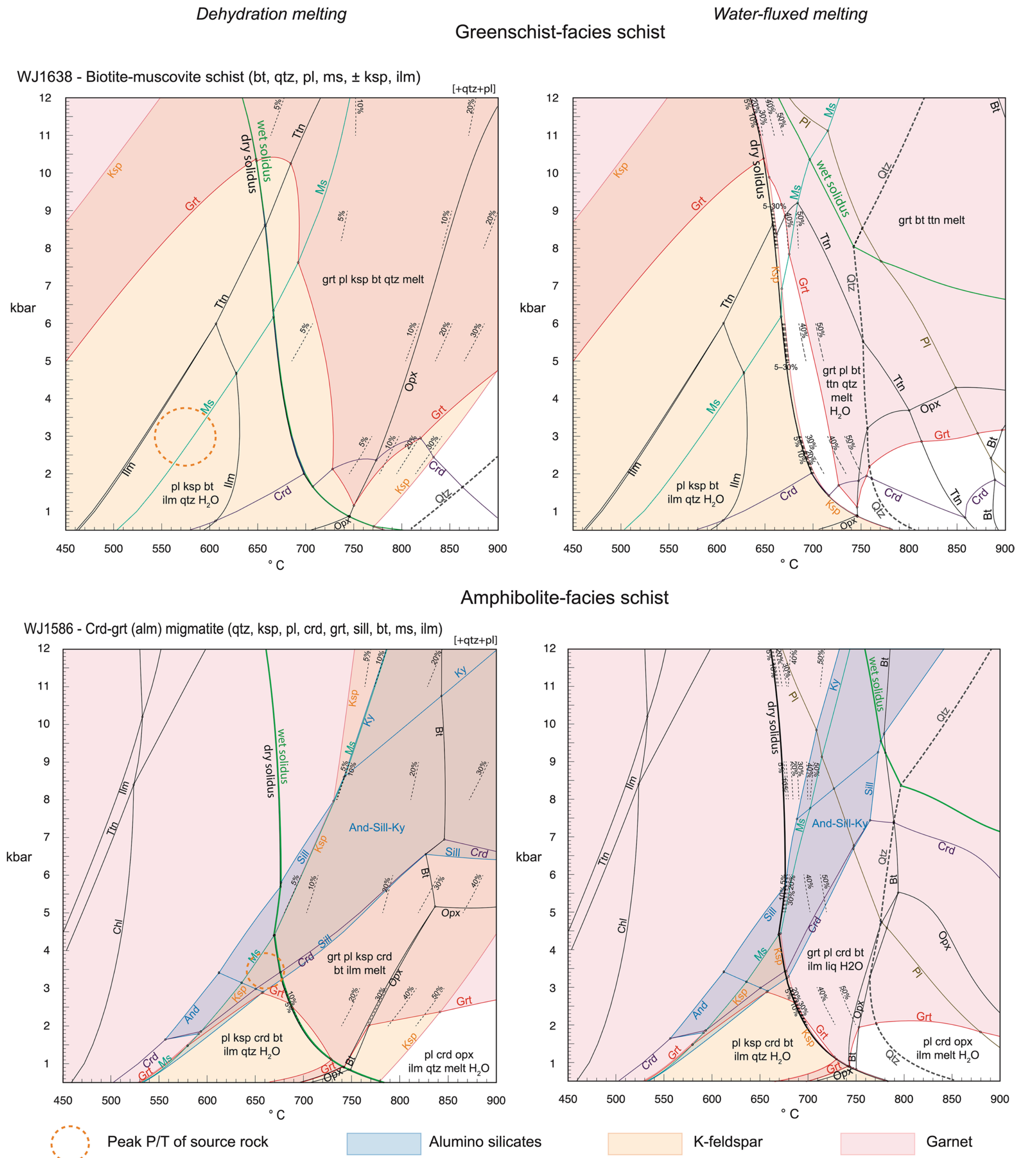

Figure 7. Pseudosections for typical greenschist and amphibolite facies metasedimentary rocks (see Figure 4a, b for others). Sections are identical below the solidus, but water was limited above the solidus for dehydration melting and kept in excess for water-fluxed melting. Dotted lines show where liquid compositions were extracted from the models. Mineral abbreviations are shown on the 'in'-side of the field boundary lines.

Results from the modelling (see below) indicated that both the Abroi Granodiorite and Wongwibinda monzogranite require some form of mixing element to account for the measured compositions of the granitoids. Isotope values of the different granitoids were compared with those of the metasedimentary rocks and known mantle values to develop criteria for various mixing scenarios.

Summary of modelled melt compositions of metasedimentary rocks of the WMC and their comparison with granitoid compositions

In the following, we summarise the results of thermodynamic modelling of melts derived from the two geochemical groups of metasedimentary rocks—less metasomatised greenschist

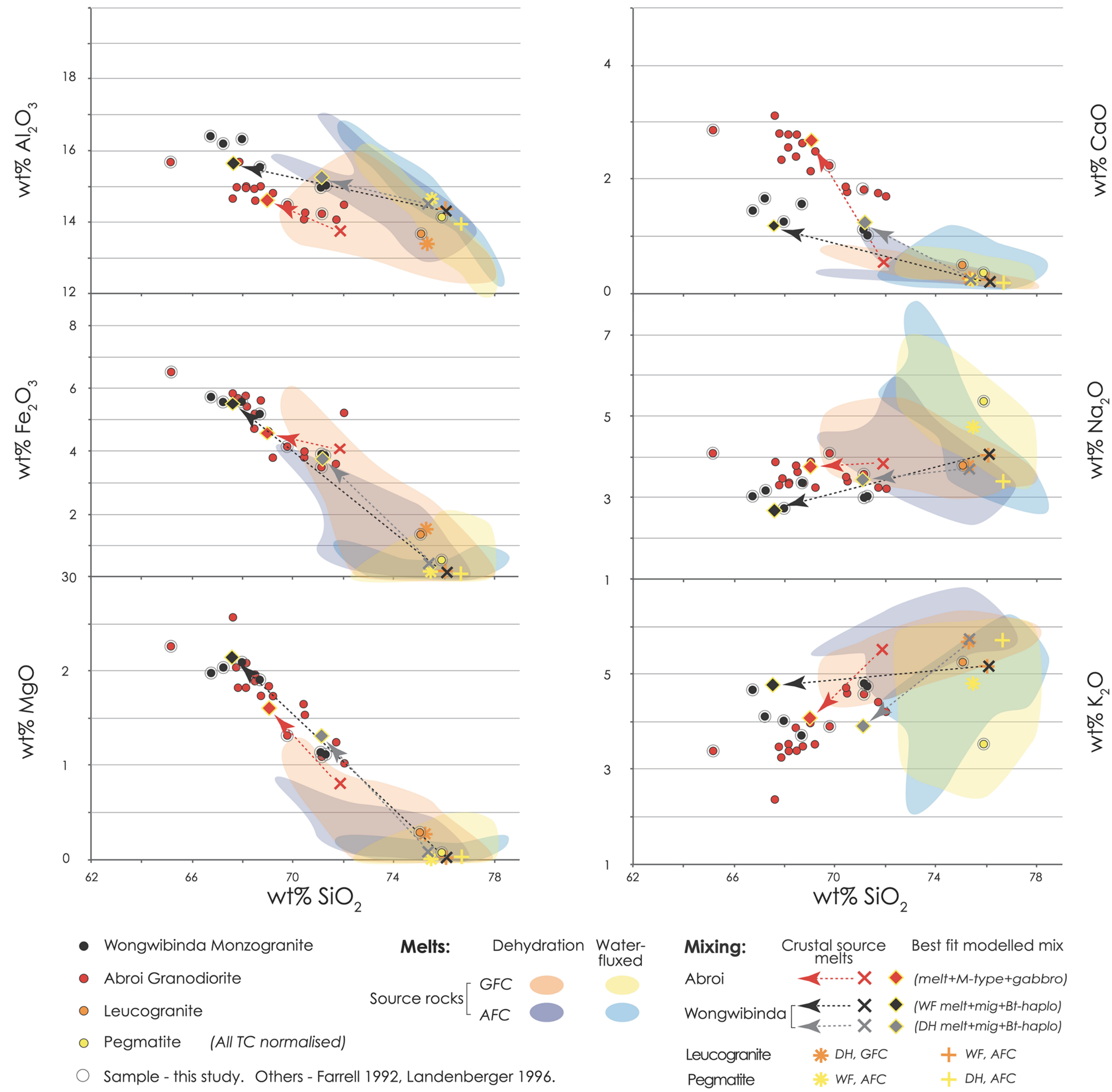

Figure 8. Harker diagrams showing range of melt compositions and TC-normalised values for the granitoids. We show the range of compositions from our study and literature for the four granitoids together with melt composition clouds of the range of partial melt compositions derived from the metasedimentary source rocks. The selected melt compositions fed into the mixing models for the Abroi Granodiorite and Wongwibinda monzogranite are shown as crosses (X) with the arrows leading to the final modelled compositions. Modelled dehydration and water-fluxed compositions for the leucogranite and pegmatite are shown as crosses (+) and asterisks (*). More details are shown on Figure S4a, b (Supplemental data). Note: DH, dehydration; GFC, greenschist facies compositions; WF, water fluxed; AFC, amphibolite facies compositions; mig, migmatite; bt, biotite; haplo, haplogranite melt.

facies rocks and more metasomatised amphibolite facies rocks—and compare these modelled partial melts with the studied granitoids. Figure 8 and Figure S4(a, b) (Supplemental data) illustrate the range of melt compositions produced under dehydration (DH) and water-fluxed (WF) conditions, with traces of melting paths under different pressure conditions also included. Notable compositional differences emerge between melts derived from the two metasedimentary groups, reflecting the influence of bulk rock composition. Melts produced from greenschist facies rock compositions, which largely preserve the chemistry of their sedimentary protoliths, are compositionally different from those generated by amphibolite facies rock compositions, which have been altered by metasomatism. These differences have important implications for the potential source characteristics of the S-type granite melts. In the following, melts from the greenschist facies rock compositions are abbreviated to GFC and from the amphibolite facies compositions to AFC.

Dehydration melting as granitoid source

(1) Partial melting of GFC source rocks produces dehydration melts with higher Fe and Mg contents and lower Si contents, particularly at higher degrees of melting (Supplemental data,

Figure S4a). (2) Metasomatised AFC source rocks produce dehydration melts with low and restricted ranges of Fe and Mg, and higher Al at a given Si content (Supplemental data, Figure S4b). The exception is sample (W0909A), which at low-pressure (3 kbar) produces 40–50% partial melts that approach the granitoid compositions for Si, Fe and Mg, although still high in Al (Supplemental data, Figure S4b). (3) Dehydration partial melts from AFC are characterised by high Si and low Ca. Low-degree partial melts are high in Na, decreasing with increasing melting, while K content is high and increases with melting. High-degree partial melts at 3 kbar for sample W0909A are outliers for these elements (Supplemental data, Figure S4b). (4) Partial melts from the GFC are low in Ca. K is high but decreases with higher pressure and moderate degrees of partial melting (Supplemental data, Figure S4a).

Dehydration partial melts that most closely match the Abroi Granodiorite are high-degree melts, although they are generally too high in Si and K, and too low in Ca, Mg and Fe (Figure 8). Two Wongwibinda monzogranite compositions align with dehydration melts from GFC at high degrees of melting at higher pressures, for Al, Fe and K only. The leucogranite falls within the melt range produced by low degrees of partial melting of both GFC and AFC (Figure 8).

WF melting as granitoid source

(1) AFC produce WF melts high in Si, with low and restricted ranges of Fe and Mg (Supplemental data, Figure S4b). (2) GFC also produce Si-rich WF melts but with slightly higher Fe and Mg contents (Supplemental data, Figure S4a). (3) WF partial melts are low in Ca, with Na increasing with pressure for all melts, decreasing with degrees of melting in AFC and increasing in GFC. K content decreases with pressure in AFC but remains stable in GFC. Partial melts from GFC show significant decreases in K with increasing degrees of partial melting and overlap with the K compositions of both the Abroi Granodiorite and Wongwibinda monzogranite. Partial melts from AFC also overlap with granitoid K compositions but fluctuate with increasing pressure and degrees of melting (Supplemental data, Figure S4a, b).

No WF partial melts closely match the Abroi Granodiorite or Wongwibinda monzogranite compositions. In contrast, the pegmatite composition fits with WF melts from both GFC and AFC.

Rationale for mixing models

Although dehydration melts from GFC most closely resemble the composition of biotite-only Hillgrove Supersuite granitoids (Figure 8) they cannot account for the required range of geochemistry. There is no clear association of any of the melt types with the Wongwibinda monzogranite. Both granitoid types are clearly S-type based on their isotopic data and high aluminium content with ASI values for the Abroi Granodiorite ranging from 0.97 to 1.13 and the Wongwibinda monzogranite ranging from 1.15 to 1.42. Thus, some form of mixing is required to attain the measured compositions of both granitoids. Conversely, no mixing is needed to explain the geochemistry of the leucogranite and pegmatites, which have ASI values of 0.97 and 1.06 respectively.

Both $^{143}Nd/^{144}Nd$ and $\delta^{18}O$ values suggest a mafic or mantle component in the Abroi magma. Conversely, the high $\delta^{18}O$ values of the Wongwibinda monzogranite, together with the similarity with the metasedimentary rocks of its $^{87}Sr/^{86}Sr$ and $^{143}Nd/^{144}Nd$ isotope ratios, preclude a non-crustal component.

Abroi Granodiorite

Several factors were considered in modelling the composition of the Abroi Granodiorite: (1) The REE values of the Abroi Granodiorite closely match those of less metasomatised greenschist facies metasedimentary rocks (Figure 5), so we focused on GFC when considering likely source rocks. (2) The $^{143}Nd/^{144}Nd$ values of the Abroi Granodiorite are higher than those of the metasedimentary rocks (Figure 6a), indicating a mafic/mantle component. This mafic component is supported by (3) the $\delta^{18}O$ values for the Abroi Granodiorite being generally lower than those of the metasedimentary rocks (Figure 6c), and (4) zircons from the Abroi Granodiorite having higher radiogenic Hf than those from the metasedimentary rocks (Craven & Daczko, 2018). Finally, (5) the high volume of Abroi Granodiorite plutons suggests high degrees of partial melting of large source regions deeper in the crust, leading us to investigate dehydration partial melts above 6 kbar and >20% melting. It is assumed that only fertile, recently deposited, crustal rocks of the Carboniferous accretionary complex form the bulk of the source for the S-type melts. The oceanic plate basaltic rocks, present in the WMC as limited amphibolites associated with meta-cherts, and more prevalent in the oldest layers of the accretionary wedge, would be the last components to experience partial melting and therefore only contribute little to the source of the S-type melts.

Based on a $\delta^{18}O$ value of 6 for mantle rocks (Rollinson, 1993) and an average $\delta^{18}O$ value of 13.3 for the Wongwibinda monzogranite samples, we calculated that approximately 30% of a mantle-derived melt mixed with a crustal melt would be required to produce the Abroi Granodiorite (average $\delta^{18}O$ of 11.1). We used in our mixing model an average M-type granitoid melt composition (Whalen *et al.*, 1987) combined with an average composition for the Days Creek Gabbro (McKibbin *et al.*, 2017), the closest Bakers Creek Supersuite pluton to the WMC. A local gabbro composition was chosen on the basis that these melts were channelled through the same deformation pathways as the Abroi Granodiorite and Wongwibinda monzogranite type melts (see following 'Granitoid suite evolution within an HTLP terrane: a model'). A suitable compositional match with the Abroi Granodiorite can be achieved through various mixes, ranging from 63 to 85% crustal melt with a 2:1 ratio of fractionated M-type melt to Days Creek Gabbro in the mantle-derived component. The crustal component in all cases forms from 30 to 40% melting of GFC at 6–9 kbar (~18–27 km depth). Figure 8 shows a 69:20:11 mix of these components, which represents a good median for the Abroi Granodiorite. The modelled mix has an ASI of 0.98, which is compatible with Abroi Granodiorite values (Supplemental data, Figure S5). This modelling indicates that the composition of the Abroi Granodiorite can be explained by magma mixing without a need to include entrained material.

Wongwibinda monzogranite

Similar factors were considered when modelling the compositions of the Wongwibinda monzogranite: (1) REE values of Wongwibinda monzogranite closely match those of the amphibolite facies metasedimentary rocks. (2) $^{143}Nd/^{144}Nd$ values of the Wongwibinda monzogranite align with those of the metasedimentary rocks. (3) The average $\delta^{18}O$ value for the Wongwibinda monzogranite (13.3) is higher than that of greenschist facies metasedimentary rocks (11.4) but is similar to amphibolite facies rocks (13.54). (4) Zircons from the Wongwibinda monzogranite have radiogenic Hf values comparable with those from the metasedimentary rocks (Jessop, 2017). (5) The low magma volumes, presence of two-micas in the granitoid (Barbarin, 1996) and its confinement to the Wongwibinda Shear Zone are consistent with WF melting. (6) Outcrop patterns suggest a melt source not significantly deeper than the current exposure levels. Pseudosection modelling indicates that peak metamorphism at Wongwibinda occurred around 3 kbar and 650 °C (Craven *et al.*, 2012), leading us to investigate melts formed at 3–6 kbar.

Isotopic values for the Wongwibinda monzogranite imply a pure crustal melt, likely formed by melting of previously metasomatised amphibolite facies metasedimentary rocks. Since none of the melt compositions obtained from the thermodynamic modelling match the granitoid composition, it suggests that the Wongwibinda monzogranite is more than just a simple melt. Entrainment of restite or peritectic phases is a possibility (Garcia-Arias & Stevens, 2017a), but the high proportion of migmatitic xenoliths in the Wongwibinda outcrops may also be obscuring the composition of the magma.

Although WF melting conditions are a possibility, we have been unable to confirm this within the scope of this study. We infer from field relationships that the melt has not travelled far from its source, limiting the depth of anatexis to around 3–6 kbar. The pattern and size of veins, dykes and plutons of Wongwibinda monzogranite also argue against high degrees of partial melting. Deformation in the shear zone would have likely promoted melt dissemination from the source.

Based on the above, we can approximate the composition of the Wongwibinda monzogranite as 45% WF, 5–10% partial melt of AFC formed at 3–6 kbar, mixed with 65% migmatite xenoliths, with loss of 20% haplogranite and associated retention of 10% biotite (Figure 8). A similar mix using a 10–20% dehydration partial melt of AFC from 3 to 6 kbar results in a composition closer to the more silica-rich phases of the granitoid (Figure 8). Many other combinations are possible, and thus the exact petrogenesis of the Wongwibinda monzogranite cannot be fully defined with the current data. Calculated ASI (1.22) for the Wongwibinda melt-mix is plotted on Figure S5 (Supplemental data).

Leucogranite

The outcrops of leucogranite on Guyra Road and adjacent Rosewood Station are the only known occurrences located at Wongwibinda to date (Figure 1). These outcrops align with a large pegmatite and may be related. Farrell (1988) suggested that leucogranitic and pegmatitic leucosomes within the migmatites were partial melts that intruded an active shear zone.

No mixing is required to match the composition of the leucogranite. Comparable compositions can be obtained with both WF and dehydration 10–20% partial melts at 3–6 kbar. Dehydration melting provides a best fit with melts from GFC, while WF melting produces more suitable compositions using melts from AFC (Figure 8).

Pegmatite

The composition of the pegmatite can be approximated by both WF and dehydration 5% partial melts of AFC at 3 kbar (Figure 8), although a WF option is preferred.

Traditionally, pegmatites are considered to form as the final volatile-rich phase of a fractionating magma. However, growing evidence indicates that some pegmatites may form as early anatectic melts (*e.g.* Shaw *et al.*, 2022). Field relationships and structural assessments at Wongwibinda suggest that the larger, undeformed pegmatites outside the shear zone were intruded early in the formation of the complex (Farrell, 1992). Pegmatites within the shear zone are abundant and display similar deformation to the host migmatites. Despite their prevalence, the pegmatites have not been studied in sufficient detail to determine whether they represent multiple phases of intrusion or a range of compositions. Our observations raise the possibility that some pegmatites may have originated from the anatexis of local country rocks.

Table 3 sets out modelled sources and mixes that can produce the measured compositions of the four granitoids from the WMC.

Table 3. Modelled melt sources and mixes for four types of granitoid from the WMC.

Melt and mix	Abroi Granodiorite	Wongwibinda monzogranite		Leucogranite		Pegmatite	
DH:WF[a]	DH	WF	DH	DH	WF	WF	DH
Pressure kbar	6–9	3–6	3–6	3–6	3–6	3	3
Partial melt %	30–40	5–10	10–20	10–20	10–20	5	5
AFC:GFC[b]	0:1	1:0	1:0	0:1	1:0	1:0	1:0
S-type %	69	45	45	100	100	100	100
M-type %	20	–	–				
Days Creek Gabbro %	11	–	–				
Haplogranite %	–	−20	−20				
Migmatite %	–	65	65				
Biotite %	–	10	10				
$\delta^{18}O$ average	11.06	13.3		13.3		–	
Zircon (Xenocryst:New)	Xenocryst + alteration	Xenocryst + alteration		Xenocryst		Xenocryst + alteration	
Zr ppm	198.8	127.0		60.5		9.4	

[a]DH, dehydration; WF, water-fluxed.
[b]AFC, amphibolite facies compositions; GFC, greenschist facies compositions.

Granitoid suite evolution within an HTLP terrane: a model

We propose a model for the formation of the four granitoid types identified within the WMC that commences with injection of pegmatites and ends with emplacement of the Abroi Granodiorite and associated biotite-only plutons. We also propose that mafic magmas of the Bakers Creek Suite signal the last phase of regional plutonism. The Wongwibinda Shear Zone acted as a major melt conduit transferring fluids and heat from the lowest crust during a period of regional extension.

The simple melt compositions of the leucogranite and pegmatites suggest that they have not travelled far from their source, nor have they been contaminated by restite or xenoliths, or lost fractionated melt. Their compositions are compatible with both WF and dehydration modelled melts produced by 10–20% partial melting at 3–6 kbar, and 5% partial melting at 3 kbar respectively. The largest pegmatite dykes are located west of the shear zone, where fracturing of strongly folded accretionary prism rocks above a west-dipping ductile shear zone likely facilitated channelling of some of the earliest low-degree partial melts directly upwards out of the shear zone.

Although the leucogranite differs from the pegmatites in terms of mineral assemblage, grainsize and chemistry, it could have been channelled from the main shear zone in a similar manner. No dates have been obtained from the leucogranite, but dating from pegmatite sample W0538 (Craven & Daczko, 2018) possibly suggests an early intrusion relative to the main pulse of S-type magmatism.

The pattern of the Wongwibinda monzogranite as apophyses within the shear zone, along with its high primary muscovite content, suggests it formed during the early stages of anatexis when aqueous fluids were relatively abundant and could drive WF melting. Initial metamorphism/metasomatism in the WMC is attributed to the advective influx of heat *via* aqueous fluids ascending the Wongwibinda Shear Zone (Craven *et al.*, 2013; Jessop, 2017). The strong association between the Wongwibinda monzogranite and the migmatites of the WMC is consistent with the granitoid having intruded during peak metamorphism. The composition of the Wongwibinda monzogranite is highly influenced by the inclusion of abundant xenolithic material and can be modelled with a mix of 45% WF 5–10% partial melt of local AFC at 3–6 kbar, 65% assimilated local migmatites, and inclusion of 10% residual biotite following the extraction of 20% haplogranite melt. The presence of quartz-rich restite within the Wongwibinda monzogranite may indicate the assimilation of earlier pegmatite veins or dykes.

The emplacement of the Abroi Granodiorite and other biotite-only Hillgrove Supersuite plutons at Wongwibinda occurred after the formation of the earlier granitoids. Large volumes of melt from deep within the crust were channelled up the Wongwibinda Shear Zone, stalling at the brittle–ductile crustal boundary. This deformation-assisted porous flow of melt likely displaced most of the earlier melts in the shear zone. The composition of the biotite-only granitoids is consistent with crustal melts produced by 30–40% dehydration partial melting of accretionary complex metasedimentary rocks at 6–9 kbar, with an admixture of ~30% mantle-derived magma.

Our work on zircons generally (Asimus et al., 2024), and within the WMC plutons in particular, supports uneasiness about dates obtained for Hillgrove Supersuite plutons (Bryant, 2017) and rocks of the Bakers Creek Supersuite. The abundance of zircon xenocrysts originally sourced from the Currabubula–Connors Arc within the metasedimentary rocks of the accretionary complex (Craven & Daczko, 2017) and subsequently within the S-type granitoids (Jeon *et al.*, 2012) can influence, and has influenced, dating of these plutons. Gabbros generally do not readily crystallise new zircon (Borisov *et al.*, 2025), and published dates for the Days Creek Gabbro (McKibbin *et al.*, 2017) are very possibly derived from variably modified zircon xenocrysts. We propose that the more mafic plutons of the Bakers Creek Supersuite, such as the Days Creek Gabbro northwest of Wongwibinda, represent the final phase of deeply sourced injection of melts with a higher mantle component. Further microstructural study of zircons in the Hillgrove and Bakers Creek Supersuite granitoids is required.

Implication of S-type granitoids in extensional HTLP terranes

The model presented may apply to other HT–LP complexes formed within extensional settings such as others found within the NEO and other Tasmanide orogens. The main variation between the complexes will reflect the level of exposure within the melt channel or 'root zone'. Binns (1966) compared the WMC with the Cooma Metamorphic Complex in the older Lachlan Orogen of the Tasmanides and concluded they were very similar. His observations infer that the exposures at Cooma are at a deeper crustal level than at Wongwibinda, which could explain the more extensive outcrop of the two-mica Cooma Granodiorite in comparison with the scattered smaller apophoses of Wongwibinda monzogranite. Richards and Collins (2002) concluded that the Cooma Metamorphic Complex formed a 'regional aureole' beneath the extensive Murrumbidgee Batholith. The north–south elongation of the Cooma Metamorphic Complex along a major fault line, however, would argue for a tectonic fluid–melt pathway.

Conclusions

The variation in granitoid types observed at Wongwibinda is characteristic of many high-temperature–low-pressure metamorphic complexes, particularly those formed in extensional environments (*e.g.* Connop *et al.*, 2024; Milord *et al.*, 2001; Wickham, 1987). Although all four types of granitoid formed during the same thermal perturbation event, they reflect distinct melting regimes and granite petrogenesis. The leucogranite and pegmatites are proposed to be the earliest melts, best preserved adjacent to the Wongwibinda Shear Zone. The Wongwibinda monzogranite may be co-genetic with these early melts, representing melts constrained within the shear zone. Field relationships and zircon dating suggest that the Abroi Granodiorite was the last of the granitoids to intrude, following the peak metamorphism of the surrounding rocks.

The leucogranite and pegmatites can be modelled with simple low-degree partial melts, consistent with their outcrop patterns. While it is plausible that the Wongwibinda monzogranite formed through WF melting of fertile Carboniferous accretionary prism metasedimentary rocks, conclusive evidence remains elusive. The compositional range of the Hillgrove Supersuite plutons—Abroi Granodiorite, Rockvale Monzogranite and Tobermory Monzogranite—can be explained by a simple mixture of mantle-derived melt mixed with a dehydration anatectic melt. While this geochemical-isotopic solution is non-unique, other alternatives such as a contribution from partial melting of I-type crust should be explored in future research.

Acknowledgements

The authors would like to thank the landholders in the Wongwibinda area for kindly providing access to their properties. Dr Terry Farrell has generously provided both samples and data collected for his PhD thesis, and these have greatly enhanced this study. Dr Bill Landenberger is also thanked for freely supplying both major, trace and isotope data and advice on isotope calculations, and Dr Richard Flood is thanked for critical assessment and adding his vast knowledge of NEO granites in discussions about the topic of this paper. Reviewers Dr Evan Leitch and Dr Colleen Bryant are thanked for their valuable input. Dr Bryant has been particularly helpful in pointing out issues with isotopes and magma mixing, and her input has greatly enhanced the document. Data collected by Macquarie University Honours students Cara Danis, Elizabeth Teague and Cait Stuart are included in this paper and attributed to them in the Supplemental data (File S1). They are thanked for their contributions, as are the staff of the laboratories at Macquarie and the University of New South Wales who processed the XRF, ICPMS and TIMS isotopic data.

Disclosure statement

No potential conflict of interest was reported by the author(s).

Funding

The majority of this work was undertaken as part of PhD research under an APA scholarship.

ORCID

K. Jessop http://orcid.org/0000-0001-6921-3942
N. R. Daczko http://orcid.org/0000-0002-3737-3818
S. Piazolo http://orcid.org/0000-0001-7723-8170

Data availability statement

Files with additional text, figures and tables are included as Supplemental data (File 1, methods and additional figures; Files 2 and 3, geochemical data).

References

Appleby, S., Gillespie, M. R., Graham, C. M., Hinton, R. W., Oliver, G. J. H., & Kelly, N. M. (2010). Do S-type granites commonly sample infracrustal sources? New results from an integrated O, U–Pb and Hf isotope study of zircon. *Contributions to Mineralogy and Petrology*, *160*(1), 115–132. https://doi.org/10.1007/s00410-009-0469-3

Asimus, J. L., Daczko, N. R., Gazi, J., Ezad, I. S., Belousov, I., Rodemann, T., Halpin, J. A., & Piazolo, S. (2024). Experimental replacement of Zircon by melt-mediated coupled-dissolution-precipitation causes dispersion in U–Pb ages. *Journal of Metamorphic Geology*, *42*(9), 1179–1195. https://doi.org/10.1111/jmg.12795

Barbarin, B. (1996). Genesis of the two main types of peraluminous granitoids. *Geology*, *24*(4), 295–298. https://doi.org/10.1130/0091-7613(1996)024%3C0295:GOTTMT%3E2.3.CO;2

Binns, R. A. (1966). Granitic intrusions and regional metamorphic rocks of Permian age from the Wongwibinda district, north-eastern New South Wales. *Journal and Proceedings of the Royal Society of New South Wales*, *99*, 5–36. https://doi.org/10.5962/p.360883

Binns, R. A., & Richards, J. R. (1965). Regional metamorphic rocks of Permian age from the New England district of New South Wales. *Australian Journal of Science*, *27*, 233.

Bonin, B., Janoušek, V., & Moyen, J-F. (2020). Chemical variation, modal composition and classification of granitoids. *Geological Society, London, Special Publications*, *491*(1), 9–51. https://doi.org/10.1144/SP491-2019-138

Borisov, A., Aranovich, L., & Antoshechkina, P. (2025). Zircon solubility in silicate melts: New empirical models and thermodynamics. *Chemical Geology*, *679*, 122682. https://doi.org/10.1016/j.chemgeo.2025.122682

Brown, C. R., Yakymchuk, C., Brown, M., Fanning, C. M., Korhonen, F. J., Piccoli, P. M., & Siddoway, C. S. (2016). From source to sink: Petrogenesis of Cretaceous anatectic granites from the Fosdick migmatite–granite complex, West Antarctica. *Journal of Petrology*, *57*(7), 1241–1278. https://doi.org/10.1093/petrology/egw039

Brown, M. (2013). Granite: From genesis to emplacement. *Geological Society of America Bulletin*, *125*(7-8), 1079–1113. https://doi.org/10.1130/B30877.1

Bryant, C. J. (2017). *A compendium of granites of the southern New England Orogen, eastern Australia* (2017/0408). Report of the Geological Survey of New South Wales.

Cawood, P. A. (1982). Structural relations in the subduction complex of the Paleozoic New England Fold Belt, eastern Australia. *The Journal of Geology*, *90*(4), 381–392. https://doi.org/10.1086/628692

Cawood, P. A. (1983). Modal composition and detrital clinopyroxene geochemistry of lithic sandstones from the New England Fold Belt (east Australia): A Paleozoic forearc terrane. *Geological Society of America Bulletin*, *94*(10), 1199–1214. https://doi.org/10.1130/0016-7606(1983)94%3C1199:MCADCG%3E2.0.CO;2

Cawood, P. A. (1984). A geochemical study of metabasalts from a subduction complex in eastern Australia. *Chemical Geology*, *43*(1-2), 29–47. https://doi.org/10.1016/0009-2541(84)90139-6

Cawood, P. A., Leitch, E. C., Merle, R. E., & Nemchin, A. A. (2011). Orogenesis without collision: Stabilizing the Terra Australis accretionary orogen, eastern Australia. *Geological Society of America Bulletin*, *123*(11-12), 2240–2255. https://doi.org/10.1130/B30415.1

Chappell, B. W., & White, A. J. R. (1974). Two contrasting granite types. *Pacific Geology*, *8*, 173–174.

Clemens, J. D. (2014). Element concentrations in granitic magmas: Ghosts of textures past? *Journal of the Geological Society of London*, *171*(1), 13–19. https://doi.org/10.1144/jgs2013-008

Clemens, J. D., & Stevens, G. (2012). What controls chemical variation in granitic magmas? *Lithos*, *134–135*, 317–329. https://doi.org/10.1016/j.lithos.2012.01.001

Collins, W. J., & Richards, S. W. (2008). Geodynamic significance of S-type granites in circum-Pacific orogens. *Geology*, *36*(7), 559–562. https://doi.org/10.1130/G24658A.1

Connop, C. H., Smye, A. J., Garber, J. M., & Mittal, T. (2024). Heat sources for Variscan high-temperature-low-pressure metamorphism: Petrochronological constraints from the Trois Seigneurs massif, French Pyrenees. *Journal of Metamorphic Geology*, *42*(6), 867–907. https://onlinelibrary.wiley.com/doi/pdf/10.1111/jmg.12775 https://doi.org/10.1111/jmg.12775

Craven, S. J. (2015). *The evolution of the Wongwibinda high-T–low-P metamorphic complex* [Unpublished PhD thesis]. Macquarie University.

Craven, S. J., & Daczko, N. R. (2017). The Keepit arc: Provenance of sedimentary rocks in the central Tablelands Complex, southern New England Orogen, Australia, as recorded by zircon. *Australian Journal of Earth Sciences*, *64*(3), 401–418. https://doi.org/10.1080/08120099.2017.1297329

Craven, S. J., & Daczko, N. R. (2018). High-temperature–low-pressure metamorphism and the production of S-type granites of the Hillgrove Supersuite, southern New England Orogen, NSW, Australia. *Australian Journal of Earth Sciences*, *65*(2), 191–207. https://doi.org/10.1080/08120099.2018.1425908

Craven, S. J., Daczko, N. R., & Halpin, J. A. (2012). Thermal gradient and timing of high-T–low-P metamorphism in the Wongwibinda Metamorphic Complex, southern New England Orogen, Australia. *Journal of Metamorphic Geology*, *30*(1), 3–20. https://doi.org/10.1111/j.1525-1314.2011.00949.x

Craven, S. J., Daczko, N. R., & Halpin, J. A. (2013). High-T–low-P thermal anomalies superposed on biotite-grade rocks, Wongwibinda Metamorphic Complex, southern New England Orogen, Australia: Heat advection by aqueous fluid? *Australian Journal of Earth Sciences*, *60*(5), 621–635. https://doi.org/10.1080/08120099.2013.814590

Daczko, N. R., Elliott, V., Piazolo, S., & Hao, K. (2024). Zircon coupled dissolution-precipitation replacement during melt-rock interaction modifies chemical signatures resulting in misleading ages. *Journal of Metamorphic Geology*, *42*(9), 1197–1214.), https://doi.org/10.1111/jmg.12796

Danis, C. (2007). *The Wongwibinda Complex, New England Fold Belt: A tilted low-P high-T terrane?* [Unpublished BSc honours thesis]. Macquarie University.

Danis, C. R., Daczko, N. R., Lackie, M. A., & Craven, S. J. (2010). Retrograde metamorphism of the Wongwibinda Complex, New England Fold Belt and the implications of 2.5 D subsurface geophysical structure for the metamorphic history. *Australian Journal of Earth Sciences*, *57*(3), 357–375. https://doi.org/10.1080/08120091003678361

Farina, F., Stevens, G., & Villaros, A. (2012). Multi-batch, incremental assembly of a dynamic magma chamber: The case of the Peninsula pluton granite (Cape Granite Suite, South Africa). *Mineralogy and Petrology*, *106*(3-4), 193–216. https://doi.org/10.1007/s00710-012-0224-8

Farmer, M. (2017). *Migmatite delineates zones of melt flux through the upper crust, Wongwibinda, NSW* [Unpublished MSc thesis]. Macquarie University.

Farrell, T. R. (1988). Structural geology and tectonic development of the Wongwibinda Metamorphic Complex. In J. D. Kleeman (Ed.), *New England Orogen tectonics and metallogenesis* (pp. 117–124). University of New England.

Farrell, T. R. (1992). *Deformation, metamorphism and migmatite genesis in the Wongwibinda Metamorphic Complex, Eastern Australia* [Unpublished PhD Thesis]. University of Newcastle.

Flood, R. H., & Shaw, S. E. (1977). Two "S-type" granite suites with low initial $^{87}Sr/^{86}Sr$ ratios from the New England Batholith, Australia. *Contributions to Mineralogy and Petrology*, *61*(2), 163–173. https://doi.org/10.1007/BF00374365

Fowler, M. B., Henney, P. J., Darbyshire, D. P. F., & Greenwood, P. B. (2001). Petrogenesis of high Ba–Sr granites: The Rogart pluton, Sutherland. *Journal of the Geological Society*, *158*(3), 521–534. https://doi.org/10.1144/jgs.158.3.521

Gao, L-E., & Zeng, L. (2014). Fluxed melting of metapelite and the formation of Miocene high-CaO two-mica granites in the Malashan gneiss dome, southern Tibet. *Geochimica et Cosmochimica Acta*, *130*, 136–155. https://doi.org/10.1016/j.gca.2014.01.003

Gao, L-E., Zeng, L., & Asimow, P. D. (2017). Contrasting geochemical signatures of fluid-absent versus fluid-fluxed melting of muscovite in metasedimentary sources: The Himalayan leucogranites. *Geology*, *45*(1), 39–42. https://doi.org/10.1130/G38336.1

García-Arias, M. (2020). The never-ending pursuit of a definitive chemical classification system for granites. *Journal of Geosciences*, *65*(4), 221–227. https://doi.org/10.3190/jgeosci.313

Garcia-Arias, M., & Stevens, G. (2017a). Phase equilibrium modelling of granite magma petrogenesis: A. An evaluation of the magma compositions produced by crystal entrainment in the source. *Lithos*, *277*, 131–153. https://doi.org/10.1016/j.lithos.2016.09.028

Garcia-Arias, M., & Stevens, G. (2017b). Phase equilibrium modelling of granite magma petrogenesis: B. An evaluation of the magma compositions that result from fractional crystallization. *Lithos*, *277*, 109–130. https://doi.org/10.1016/j.lithos.2016.09.027

Hensel, D., McCulloch, M. T., & Chappell, B. W. (1985). The New England Batholith: Constraints on its derivation from Nd and Sr isotopic studies of granitoids and country rocks. *Geochimica et Cosmochimica Acta*, *49*(2), 369–384. https://doi.org/10.1016/0016-7037(85)90030-4

Holland, T. J. B., & Powell, R. (2011). An improved and extended internally consistent thermodynamic dataset for phases of petrological interest, involving a new equation of state for solids. *Journal of Metamorphic Geology*, *29*(3), 333–383. https://doi.org/10.1111/j.1525-1314.2010.00923.x

Jeon, H., Williams, I. S., & Chappell, B. W. (2012). Magma to mud to magma: Rapid crustal recycling by Permian granite magmatism near the eastern Gondwana margin. *Earth and Planetary Science Letters*, *319-320*, 104–117. https://doi.org/10.1016/j.epsl.2011.12.010

Jessop, K. (2017). *The role of aqueous fluids in regional-style HTLP metamorphism* [Unpublished PhD thesis]. Macquarie University.

Jessop, K., Daczko, N. R., & Piazolo, S. (2019). Tectonic cycles of the New England Orogen, Eastern Australia: A review. *Australian Journal of Earth Sciences*, *66*(4), 459–496. https://doi.org/10.1080/08120099.2018.1548378

Jessop, K., Daczko, N. R., & Piazolo, S. (2020). Two belts of HTLP sub-regional metamorphism in the New England Orogen, Eastern Australia: Occurrence and characteristics exemplified by the Wongwibinda Metamorphic Complex. *Australian Journal of Earth Sciences*, *67*(4), 479–507. https://doi.org/10.1080/08120099.2019.1698275

Johannes, W., & Holtz, F. (2012). *Petrogenesis and experimental petrology of granitic rocks*. Springer Science & Business Media.

Kent, A. J. R. (1994). Geochronology and geochemistry of Palaeozoic intrusive rocks in the Rockvale region, southern New England Orogen, New South Wales. *Australian Journal of Earth Sciences*, *41*(4), 365–379. https://doi.org/10.1080/08120099408728145

Koblinger, B. M., & Pattison, D. R. M. (2017). Crystallization of heterogeneous pelitic migmatites: Insights from thermodynamic modelling. *Journal of Petrology*, *58*(2), 297–326. https://doi.org/10.1093/petrology/egx017

Korsch, R. J., Totterdell, J. M., Cathro, D. L., & Nicoll, M. G. (2009). Early Permian East Australian Rift System. *Australian Journal of Earth Sciences*, *56*(3), 381–400. https://doi.org/10.1080/08120090802698703

Landenberger, B. (1996). *Petrogenesis and tectono-magmatic evolution of S-type and A-type granites in the New England Batholith* [Unpublished PhD Thesis]. University of Newcastle.

Landenberger, B. (2001). Sediment maturity and the fertility of S-type granite sources: A lesson from the Hillgrove Suite, New England Batholith. In *S-type Granites and Related Rocks*. AGSO Record 2001/2 (pp. 71–72). Allan White Symposium.

Landenberger, W., McKibbin, S., & Collins, W. (2010). Genesis and age of magmas of the Hillgrove Batholith, southern New England Orogen. In S. Buckman & P. L. Blevin (Eds.), *New England Orogen 2010 Conference* (pp. 200–206). University of New England.

Li, R., Collins, W. J., Yang, J-H., Blereau, E., & Wang, H. (2021). Two-stage hybrid origin of Lachlan S-type magmas: A re-appraisal using isotopic microanalysis of lithic inclusion minerals. *Lithos*, *402-403*, 106378. https://doi.org/10.1016/j.lithos.2021.106378

Li, S., Chung, S-L., Wang, T., Wilde, S. A., Chu, M-F., Pang, C-J., & Guo, Q-Q. (2018). Water-fluxed crustal melting and petrogenesis of large-scale Early Cretaceous intracontinental granitoids in the southern Great Xing'an Range, North China. *Geological Society of America Bulletin*, *130*(3-4), 580–597. https://doi.org/10.1130/B31771.1

Mayne, M. J., Stevens, G., & Moyen, J-F. (2020). A phase equilibrium investigation of selected source controls on the composition of melt batches generated by sequential melting of an average metapelite. *Geological*

Society, London, Special Publication, *491*, 223–241. https://doi.org/10.1144/SP491-2018-121

McKibbin, S. J. (2006). *Origin, evolution and tectonic implications of Late-Carboniferous mafic magmas in the Southern New England Fold Belt* [Unpublished BSc honours thesis]. University of Newcastle.

McKibbin, S. J., Landenberger, B., & Fanning, M. C. (2017). First magmatism in the New England Orogen, Australia: Forearc and arc-backarc components in the Bakers Creek Suite gabbros. *Solid Earth*, *8*(2), 421–434. https://doi.org/10.5194/se-8-421-2017

Milord, I., Sawyer, E. W., & Brown, M. (2001). Formation of diatexite migmatite and granite magma during anatexis of semi-pelitic metasedimentary rocks: An example from St. Malo, France. *Journal of Petrology*, *42*(3), 487–505. https://doi.org/10.1093/petrology/42.3.487

Patiño Douce, A. E., & Harris, N. (1998). Experimental constraints on Himalayan anatexis. *Journal of Petrology*, *39*(4), 689–710. https://doi.org/10.1093/petroj/39.4.689

Pavan, M., Moraes, R., & Sawyer, E. (2021). Changes in the composition of anatectic melt and its complementary residue by forward-modelling using THERMOCALC. *Lithos*, *396-397*, 106220. https://doi.org/10.1016/j.lithos.2021.106220

Phillips, G., Landenberger, B., & Belousova, E. A. (2011). Building the New England Batholith, eastern Australia—Linking granite petrogenesis with geodynamic setting using Hf isotopes in zircon. *Lithos*, *122*(1-2), 1–12. https://doi.org/10.1016/j.lithos.2010.11.005

Powell, R., Guiraud, M., & White, R. W. (2005). Truth and beauty in metamorphic phase-equilibria: Conjugate variables and phase diagrams. *The Canadian Mineralogist*, *43*(1), 21–33. https://doi.org/10.2113/gscanmin.43.1.21

Powell, R., Holland, T. J. B. H., & Worley, B. (1998). Calculating phase diagrams involving solid solutions via non-linear equations, with examples using THERMOCALC. *Journal of Metamorphic Geology*, *16*(4), 577–588. https://doi.org/10.1111/j.1525-1314.1998.00157.x

Richards, S. W., & Collins, W. J. (2002). The Cooma Metamorphiic Complex, a low-P, high-T (LPHT) regional aureole beneath the Murrumbidgee Batholith. *Journal of Metamorphic Geology*, *20*(1), 119–134. https://doi.org/10.1046/j.0263-4929.2001.00360.x

Rollinson, H. (1993). *Using geochemical data: Evaluation, presentation, interpretation*. Pearson Education, Prentice Hall.

Rosenbaum, G., Li, P., & Rubatto, D. (2012). The contorted New England Orogen (eastern Australia): New evidence from U–Pb geochronology of early Permian granitoids. *Tectonics*, *31*(1), TC1006. https://doi.org/10.1029/2011tc002960

Sawyer, E. W., Cesare, B., & Brown, M. (2011). When the continental crust melts. *Elements*, *7*(4), 229–234. https://doi.org/10.2113/gselements.7.4.229

Shaw, R. A., Goodenough, K. M., Deady, E., Nex, P., Ruzvidzo, B., Rushton, J. C., & Mounteney, I. (2022). The magmatic–hydrothermal transition in lithium pegmatites: Petrographic and geochemical characteristics of pegmatites from the Kamativi area, Zimbabwe. *The Canadian Mineralogist*, *60*(6), 957–987. https://doi.org/10.3749/canmin.2100032

Shaw, S. E., & Flood, R. H. (1981). The New England Batholith, eastern Australia: Geochemical variations in time and space. *Journal of Geophysical Research: Solid Earth*, *86*(B11), 10530–10544. https://doi.org/10.1029/JB086iB11p10530

Shaw, S. E., Flood, R. H., & Pearson, N. J. (2011). The New England Batholith of eastern Australia: Evidence of silicic magma mixing from zircon $^{176}Hf/^{177}Hf$ ratios. *Lithos*, *126*(1-2), 115–126. https://doi.org/10.1016/j.lithos.2011.06.011

Spier, C. A., Daczko, N. R., & Zhou, R. (2024). Zircon coupled dissolution-precipitation textures distinguish xenocrystic cargo from rare magmatic zircon in the Paleoarchean Bacuri Mafic-Ultramafic layered Complex, Brazil. *Precambrian Research*, *404*, 107342. https://doi.org/10.1016/j.precamres.2024.107342

Stuart, C. A. (2012). *Aqueous fluid advection: A plausibe mechanism for heating the shallow crust to form HTLP metamorphic belts* [Unpublished BSc honours thesis]. Macquarie University.

Teague, E. (2010). *A geochronological assessment into the evolution of the Wongwibinda Complex, Southern New England Fold Belt* [Unpublished BSc honours thesis]. Macquarie University.

Villaros, A. (2010). *Petrogenesis of S-type granites: The example of the Cape Granite Suite* [Unpublished PhD thesis]. University of Stellenbosch.

Weinberg, R. F., & Hasalová, P. (2015). Water fluxed melting of the continental crust: A review. *Lithos*, *212–215*, 158–188. https://doi.org/10.1016/j.lithos.2014.08.021

Whalen, J. B., Currie, K. L., & Chappell, B. W. (1987). A-type granites: Geochemical characteristics, discrimination and petrogenesis. *Contributions to Mineralogy and Petrology*, *95*(4), 407–419. https://doi.org/10.1007/BF00402202

White, A. J. R., & Chappell, B. W. (1988). Some supracrustal (S-type) granites of the Lachlan Fold Belt. *Earth and Environmental Science Transactions of the Royal Society of Edinburgh*, *79*(2-3), 169–181. https://doi.org/10.1130/SPE272-p1

Wickham, S. M. (1987). Crustal anatexis and granite petrogenesis during low-pressure regional metamorphism: The Trois Seigneurs Massif, Pyrenees, France. *Journal of Petrology*, *28*(1), 127–169. https://doi.org/10.1093/petrology/28.1.127

Zhang, Q-Q., Gao, X-Y., & Zheng, Y-F. (2023). The different responses of trace elements to equilibrium and disequilibrium melting: Implications for crustal differentiation and granite compositions. *Chemical Geology*, *625*, 121426. https://doi.org/10.1016/j.chemgeo.2023.121426